Texas A&M University
Mechanical Engineering Department
Turbomachinery Laboratory
Tribology Group

A MODEL FOR THE ANALYSIS OF FLOW STARVED TILTING PAD THRUST BEARINGS

TRC-B&C-02-20

A Report to the Turbomachinery Research Consortium

By
Rasool Koosha
Forner Graduate Research Assistant

Luis San Andrés
Mast-Childs Chair Professor
Principal Investigator

June 2020

TRC Project, TEES # 28-258124-00022

EXECUTIVE SUMMARY

Work in 2020 implements a flow starvation model into the XLTHRUSTBEARING® computational analysis tool to deliver static and dynamic load performance predictions for tilting pad thrust bearings (TPTB) operating under lubricant flow starvation. The model takes the supply flow rate as an input to determine the temperature of the lubricant entering a thrust pad and the prediction of the pressure and temperature fields. Under a starved flow condition, the analysis iteratively reduces the effective arc length of a wetted pad until matching the available flow. As the XLTHRUSTBEARING® is a multiple pad predictive tool able to account for thrust collar misalignment, a sound model sets the distribution of the supplied flow into each of the bearing pads as based on their demand for fresh flow.

The analysis considers an example eight pad thrust bearing with ID= 122 mm and OD=267 mm, 38° pad arc length, operating at 4 krpm and 10 krpm ($R_o\Omega$ = 54 m/s and 135m/s), and under a specific load per pad from 0.7 MPa to 3.4 MPa. Predictions from the model are benchmarked against measured lubricant exit temperature rise and (mid radius) subsurface temperature rise at the pad leading edge, center, and trailing edge. The predictions agree with the test data with a maximum difference of 4 °C for the lubricant exit temperature, and 11 °C (14% with respect to measurements) for the pads temperature rise.

Next, predictions follow for the example bearing operating at 4 krpm and under a specific load per pad of 1, 2 and 3 MPa and with a supply flow rate ranging from 150% to only 25% of the nominal flow rate. Under the heavy load of 3 MPa, the pad subsurface temperature almost doubles as the supply flow rate decreases whereas the minimum film thickness decreases by ~75%. A flow starvation also results in a significant increase in the predicted bearing axial stiffness while the damping coefficient decreases by half.

TABLE OF CONTENTS

LIST OF FIGURES

NOMENCLATURE

c_P	Lubricant specific heat [J/kg ˚C].
C_i	Supply flow rate ratio to each pad of a bearing.
C_z	Bearing axial damping coefficient [Ns/m].
e_c	Axial location of thrust collar [m].
e_P	Axial location of pivot tip [m].
E	Material elastic modulus [Pa].
G, H_r, H_θ	Turbulent flow functions, Eqn. (2).
h	Fluid film thickness [m].
K_z	Bearing axial stiffness coefficients [N/m].
N_p	Number of pads in a TPTB.
P	Pressure [Pa].
Pr	Prandtl number.
Pr^*	Turbulent flow Prandtl number.
Q	Flowrate [LPM].
R_i, R_o	Inner radius and outer radius of a pad [m].
(R_P, θ_P)	Radial and circumferential location of pivot [m].
t_p	Pad thickness [m].
T	Fluid film temperature [˚C].
T_p	Pad temperature [˚C].
(U, V, W)	Flow velocity components in global cylindrical coordinate system [m/s].
W_z	Applied axial load [N].
Z_{XY}	Complex dynamic stiffness coefficient (X=z, γ, ξ and Y = e_c, e_p, α, β).
(α, β)	Pad tilt angles around (γ, ξ) axes [rad].
α_{TV}	Lubricant temperature-viscosity coefficient [1/˚C].
α_T	Material isotropic thermal expansion coefficient [1/˚C].
ϵ_m	Eddy viscosity for momentum [m^2/s].
ϵ_H	Eddy viscosity for heat [m^2/s].
θ_t	Circumferential location of trailing edge in global coordinate system [rad].
θ_l	Circumferential location of leading edge in global coordinate system [rad].
λ	Heat convection coefficient [W/m^2 ˚C].
μ	Lubricant dynamic viscosity [Pa.s].
ν	Lubricant kinematic viscosity (cSt).
υ	Poisson ratio.
ρ	Lubricant density [kg/m^3]
κ	Lubricant conductivity coefficient [W/m C].
Ω	Shaft angular speed [rad/s].

ω	Excitation frequency [rad/s].

Matrices

$\mathbf{C}$	Damping coefficients.
$\mathbf{F}$	Force Vector.
$\mathbf{K}$	Stiffness coefficients.
$\mathbf{K}^e$	Element structure stiffness for FE model.
$\mathbf{Z}$	Complex stiffness coefficients.
$\boldsymbol{\sigma}$	Stress tensor.
$\boldsymbol{\varepsilon}$	Strain tensor.

Subscripts

BF	Back flow
h	Bearing housing
in	Inner radius
LE	Leading edge
out	Outer radius
p	Pad
P	Pivot
TE	Trailing edge
Su	Supply

Coordinate Systems

(x,y,z)	Cartesian coordinate system with origin at the center of bearing housing surface .
(r,θ,z)	Cylindrical coordinate system with origin at the center of bearing housing surface.

Abbreviation

FEM	Finite element method.
ID	Inner diameter.
OD	Outer diameter.
LPM	Liter per minute.
TEHD	Thermo-elasto-hydrodynamic.
TPJB	Tilting pad journal bearing.
TB	Thrust bearing.
TPTB	Tilting pad thrust bearing.
RPM	Repeat per minute.

INTRODUCTION

Thrust Bearings (TBs) control rotor axial position in rotating machinery, and when properly lubricated, reduce drag power losses and eliminate contact and wear of material surfaces. Figure 1 depicts a schematic view of a tilting pad thrust bearing (TPTB) with exaggerated pad tilt angles and fluid film thickness. A TPTB consists of a series of pads placed on a bearing housing free to tilt where a thrust collar attached to the shaft rotates on top of them. Feed ports or orifices deliver fresh oil into grooves between bearing pads to mix with the hot oil carried by the rotating thrust collar. The ensuing flow enters the leading edge of a bearing pad to build a pressure field able to withstand an applied load while carrying away heat generated by viscous drag power losses on the pad lubricated area.

Lubricant circulation is a major cost during the operation life and maintenance of fluid film bearings. An ancillary oil supply system (sump, pumps, filters and piping) must provide adequate flow and pressure into a bearing, whereas an oil evacuation system returns the hot oil for deaeration, cooling and storage in a sump. Industrial practice often reduces the required flow to fully wet the bearing film lands in a planned effort to reduce drag power losses and operation costs, and to extend the life of the lubricant while reducing oil churning losses. The practice, if not properly assessed, can lead to excessive temperature rises of the lubricant and pad surfaces, overly thin film thickness, and the risk of lubricant varnishing and coking with failure of the Babbitted pad surfaces (San Andrés et al. [1] and Gregory [2]).

The major question is how low a supplied lubricant flow can be to warrant safe and reliable operation while ensuring the integrity of the mechanical components and demonstrating a sizable reduction in drag power loss.

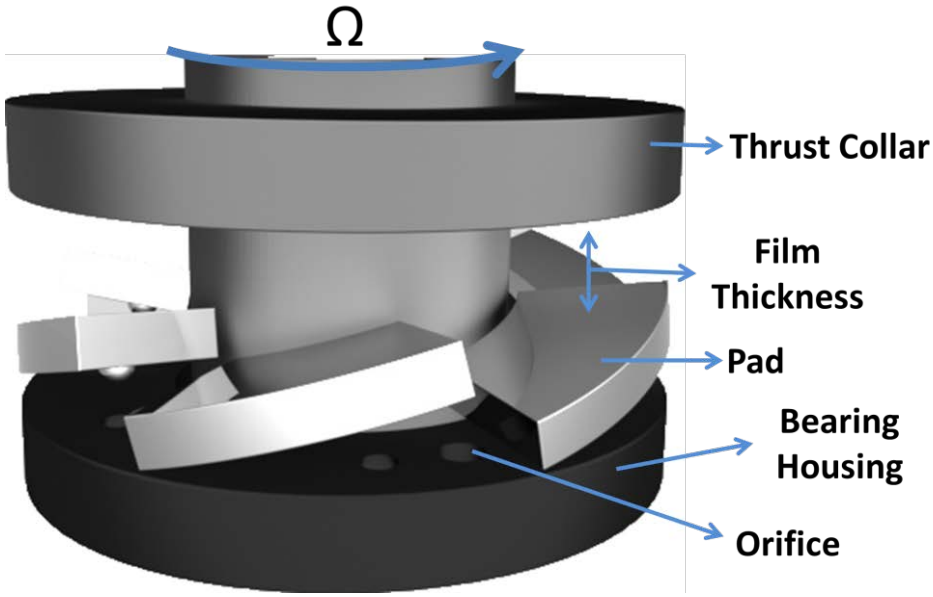

Fig. 1: Schematic view of a tilting pad thrust bearing (Film thickness and pad tilts exaggerated). Ω is the rotor speed.

Under a starved flow operation, the supply flow rate is not enough to fully fill in the gap over an entire pad surface. Thus, the fluid film forms later (not at the leading edge) and this makes for an effectively shorter pad arc length (Hashimoto [3]). In an over-flooded flow condition, the bearing is fed with a supply flow rate larger than the one needed, i.e. the one determined by predictions. Consequently, the additional flow displaces to the gap between the sides of the pads and the end seals and falls under the pads to increase oil churning power losses [1] while also aiding to transfer heat away from bearing pads.

In an effort to extend the current analysis to account for the supply flow rate as an input variable, a model for operation under either a flow starvation or an over-flooded conditions helps better evaluate a TPTB performance toward reducing both the drag power loss and the oil flow consumption.

Work here implements a flow starvation model introduced by San Andres et al. [1] into the current XLTHRUSTBEARING® analysis tool to deliver static and dynamic load performance predictions for TPTBs as a function of the supply flow rate. Presently, XLTHRUSTBEARING® is an analysis tool for both regular (non-equalizing) and self-equalizing (multiple-pad) TPTBs with an option to account for thrust collar misalignment. This report further adopts a flow thermal mixing model advanced by Abdollahi and San Andrés [4] to determine the portion of supply flow rate

delivered into each feed groove, and consequently estimate the inlet temperature for each pad. Different to a single-pad analysis tool that assumes identical operating conditions for all pads, a multiple-pad analysis tool recognizes the variation of applied load among the pads due to thrust collar misalignment and runs individual analyses specific to each pad condition. Thrust collar misalignment, besides applying bending moments on the rotating structure, also imposes a distinct flow requirement for each feed groove in a bearing. Hence, the overall supply flow no longer divides equally among the bearing feed grooves and the inlet lubricant temperature varies from pad to pad.

1. REVIEW OF PAST WORK

Bielec and Leopard (1969) [5] measure temperature rise below a pad surface in an eight-pad steel-Babbitted tilting pad thrust bearing (TPTB) with 124 mm in outer diameter (OD), 68 mm in inner diameter (ID). The bearing operates under a specific load[1] ranging from 1 MPa to 6 MPa per pad and at a rotor speed between 2 krpm and 12 krpm (maximum surface speed[2] ΩR_o = 13 m/s to 78 m/s). At 8 krpm and under 4.2 MPa/pad specific load, the measured pad peak subsurface temperature rise constantly increases from 70 ºC to 90 ºC as the supply flow rate decreases from over 100 liter per minute (LPM) to less than 10 LPM. The exit oil temperature rise also increases from 3 ºC to 40 ºC. The authors further evaluate a flooded lubrication system with the supply flow inlet at the bearing ID vs one with the inlet at the OD. With the supply flow inlet at the ID, the oil well distributes into the bearing grooves to fully lubricate the bearing pads. However, with the supply flow at the bearing OD, oil had to move against a centrifugal effect, induced by collar rotation, to reach the bearing pads. Therefore, the majority of the oil wetted the OD area until exiting the bearing while some inner ID areas on the pads remained denuded of oil. This finding also reveals that with a flooded lubrication method, the flow exiting a pad at the ID may enter the inlet of the downstream pads whereas the flow exiting a pad at the OD is thrown away and returns to the sump.

In 1974, Gregory [2] experimentally investigates the effect of supply flow rate on the static load performance of TPTBs. The author measures pad temperatures and drag power loss in a double-sided eight-pad bearing with 0.267 m in OD operating at a rotor speed of 4-11 krpm (ΩR_o = 55 - 154 m/s) and under a specific load up to 2.8 MPa per pad. The lubricating condition includes three supply flow rates: the manufacturer recommended flow rate (flooded), 50% above than the recommended flow rate (over-flooded), and 50% lesser than the recommended rate (starved). A double-sided TPTB consists of bearings facing opposite sides of a thrust collar; one bearing acts against a primary axial load in the system (active side), while the other one takes occasional reverse-direction loads (inactive or slack-side). Gregory observes that, compared to a flooded condition, a flow starvation lessens the power loss up to 20%, while with an over-flood flow the

[1] Unit load or specific load = F_{pad}/A_{pad}, where F_{pad} [N] is the axial load on a pad and A_{pad} [m^2] is its area.
[2] The maximum surface speed of a thrust bearing equals $R_o\Omega$, where Ω is the rotor speed [rad/s] and R_o as the outer radius [m].

drag power loss increases by 30%. Nonetheless, the TPTB operating under a starved flow condition shows a higher pad temperature raise, up to 15 ºC higher than that in the flooded bearing. On the other hand, the over-flooded TPTB shows only a 5 ºC reduction in pad temperature rise. The author confirms the TPTB operates safely and remains pristine when operating with ½ the recommended flow condition. Note Gregory [2] uses a thermal balance method between the inlet and outlet flows to estimate the bearing drag power loss. San Andrés et al [6] (among many others) show such thermal balance method underestimates the bearing power loss when operating with a reduced flow rate.

Two years later (1976), Capitao at al. [7] measure pad subsurface temperature rise and drag power loss in a double-sided TPTB while operating under both laminar flow and turbulent flow conditions and with a supply flow rate ranging from 50% to 150% of the recommended magnitude. The authors test two six-pad steel-babbitted bearings, one with OD=267 mm and the other with OD=304 mm, operating under a specific load per pad ranging from 0.7 MPa to 2.8 MPa, and with the rotor turning at speeds between 4 krpm and 14 krpm (ΩR_o = 55-192 m/s for the smaller bearing, and ΩR_o = 63-218 m/s for the larger one). The measured pad temperature rise shows up to 16 ºC increase as the supply flow rate falls to 50% of the recommended magnitude. Yet, increasing the supply flow rate to 150% of recommended rate leads to a slight drop (maximum of 5 ºC) in the pad temperature rise. The bearing drag power loss substantially increases with shaft speed but shows minimal variations with the load applied on the bearing. More importantly, the measured drag power loss noticeably drops as the supply flow rate decreases, in particular on the high end of rotor speed ($\rightarrow$ 14 krpm). Note the work here also uses a thermal balance method to measure power loss.

In 1987, Artiles and Heshmat [8] theoretically study the effect of flow starvation on the static load performance of fixed geometry thrust bearings. Flow starvation is modeled by a reduction in the fluid film circumferential length, i.e. the film begins at an offset angle from the pad leading edge where the side leakage flow equals the bearing supply flow. The authors perform analysis for a fixed-geometry TB with ID/OD = 1/3, 1/2, and 2/3, pad arc length = 27º, 42º, and 57º, and an 80% taper extent, while operating with a supply flow ranging from 100% to just 10% of the nominal rate. The authors define the nominal rate as the minimum flow rate nominal to fully fill the gap between the bearing pads and the thrust collar. Predictions show bearing drag torque reduces by 90% when the supply flow decreases below 25% of the required rate. The predicted

pad temperature rise shows a constant increase as the supply flow rate decreases. The increase in pad temperature is substantially larger as the supply flow rate decreases below 40% of the nominal rate. Further, a reduction in supply flow rate below 70% of the nominal produces a significant reduction in the minimum film thickness.

In 1990, Hashimoto [3] study effects of flow starvation and over-flooded conditions on the performance of turbulent flow fixed-geometry TBs. The analysis models an over-flooded flow condition by an increase in the inlet pressure at the pads leading edge, whereas a starved flow condition produces a fluid film with a shorter circumferential length than the actual physical length of a pad. Predictions of minimum film thickness are compared against measurements for a water lubricated four-pad fixed-geometry TB with OD=80 mm operating under three supply flow conditions: starved, flooded, and over-flooded. The bearing operates at an angular speed of 19.8 krpm (ΩR_o = 83 m/s) and under a very light load of 200 N (0.08 MPa per pad). The circumferential Reynolds number[3] Re = 2000 at a pad leading edge. For the starved flow condition, the supply flow is fixed to 90% of the nominated rate while for the over-flooded condition the bearing is submerged into a bath of water. In general, there is a good agreement between predictions and measurements. Predictions show of an increase in pad inlet pressure when the supply flow rate exceeds the one needed to fill in the gap. The increase in pad inlet pressure is larger at a low speed and/or under a heavy load as the fluid film thickness decreases to increase the flow resistance. The author does not report either a measured or predicted drag power loss or a pad temperature rise.

Glavatskih et al. (2002) [9] use a thermal energy transport equation to determine the temperature of the flow entering a pad inlet for operations with flooded lubrication methods. Opposed to the conventional hot oil carry-over model [11], the proposed model does not rely on empirical parameters and has the advantage of accounting for the supply flow rate. The analysis assumes any extra supply flow, i.e., exceeding the one theoretically needed, displaces to the OD of the bearing to mix with the flow exiting the upstream pad at its OD, and eventually returns to the sump. A pad inlet flow temperature follows by balancing the heat (internal energy) going into a groove oil bath from the supply flow and the heat from the upstream pad, at both its trailing edge and ID. Heat leaves the groove as is carried by the side leakage flow into the bearing OD and by

[3] The circumferential Reynolds Number is Re=($\rho R_o \Omega h_{LE}/\mu$), where R_o is the outer radius of a pad, h_{LE} is the fluid film thickness at the pad leading edge, and ρ and μ are the fluid density and viscosity

the flow entering the leading edge of the downstream pad. The authors compare characteristic load performance measurements against predictions for a six-pad TPTB with 228 m in OD operating at a rotor speed up to 3 krpm (ΩR_o = 36 m/s) and under up to 2 MPa specific load per pad. Predictions match measurements with a maximum difference of 6 ºC in pad temperature, 1 kW (~20%) in drag power loss, and 8 μm (~10%) in fluid film thickness

In 2008, Wasilczuk and Rotta [10] use computational fluid dynamic (CFD) to model the flow in the feed groove of a large size water lubricated eight-pad bearing with 1.78 m in OD operating at 214 rpm (ΩR_o = 20 m/s) and with a supply flow rate of 1 kLPM. The film thickness is 65 μm at the upstream pad trailing edge and 175 μm at the downstream pad leading edge. With a flooded lubrication method, the analysis shows significant oil churning in the bearing grooves. However, induced by the centrifugal forces due to the thrust collar rotation, the radial component of the flow velocity is always outward in a groove, i.e. the oil only displaces from the ID toward the OD. The finding confirms the observation in prior work [5] that the oil pushed toward the bearing OD cannot reach into a downstream grooves or the next pad leading edge.

DeCamillo (2014) [11] investigates experimentally the onset and persistency of axial subsynchronous vibrations (SSV) in TPTBs while also evaluating the effectiveness of commonly used solutions in industry. The test bearings are a centrally pivoted and a 60% offset pivoted six-pad supplied with a conventional flooded lubrication system, a 60% offset six-pad TPTB configured with a leading-edge-groove (LEG) lubrication system, and a 65% offset eight-pad bearing with a LEG lubrication system. All bearings have 267 mm in OD and 133 mm in ID with 35.4 cm^2 in total pad area. The measured axial vibration show a substantial dependency on the supply flow rate for both fully flooded flow and starved flow operations. DeCamillo recommends adjusting (increasing or decreasing) the supplied flow rate to push the system axial natural frequency out of the range of operating conditions. Decreasing the pivot offset is effective to reduce the bearing axial stiffness and to lower the shaft amplitude of vibration. Most importantly, the implementation of an “O-Ring” damper proved a reliable option toward eliminating axial vibration.

In 2018, San Andrés et al. [1] present a simple flow model for prediction of the performance of tilting pad journal bearings (TPJBs) operating with flow starvation. The work aims to evaluate the onset of subsynchronous vibration (SSV) hash motions for TPJBs operating under flow starvation to describe unexpected low frequency shaft vibration reported in literature [12]. The

starved flow condition is treated in a similar manner as in prior literature [8, 13, 14], i.e. with a reduction in the pads effective arc length. Regardless of the flow condition, the supplied flow to a bearing is distributed among the pads based on a hydraulic network analogy. The authors assume the pad flow resistance remains unchanged regardless of supply flow condition. Hence, the fraction of supplied flow into each pad, as derived from the solution for the flooded condition, remains unchanged during operation under a flow starvation condition.

San Andrés et al. [1] detail load performance predictions for two journal bearing configurations. The first configuration is a load between pads (LBP) four-pad TPJB with 0.127 m in diameter operating at 5 krpm rotor speed (ΩR_s =33 m/s) and under a specific load[4] of 0.689 MPa. The second one is a (load on pads, LOP) five-pad TPJB with 0.423 m in diameter operating at 3.6 krpm rotor speed (ΩR_s = 80 m/s) and under 1.07 MPa of specific load. For both configurations, flow starvation reduces the bearing damping coefficient and which produces a higher amplitudes of frequency response functions (FRFs). Further, the LOP configuration demonstrates a relatively small stiffness and damping resistance against shaft displacements in the direction orthogonal to the load.

In 2019, Abdollahi and San Andrés [4] introduce a novel thermal and flow mixing model for feed grooves in TPJBs and aiming to rectify some limitations of a conventional hot oil carry-over coefficient model [15]. The model initially estimates a supply flow distribution among the bearing feed grooves based on each groove demand for supply flow. Then, a *groove efficiency* coefficient represents the ability of a groove to discharge the hot upstream flow and heat out of the groove and which is used to determine the side leakage flow temperature. Unlike the (empirical) hot oil carry-over coefficient, the groove efficiency coefficient is not a function of the bearing operating condition and remains constant. The fluid inlet flow and temperature at the leading edge of each bearing pad follow from balances of flow and heat in a volume enclosing the feed groove and the sides of the trailing edge of the upstream pad and the leasing edge of the downstream pad. The model includes for bearing configurations with evacuated ends (no end seals) and fully flooded (with end seals). Pad subsurface temperature rise predictions from the new model and the conventional hot oil carry-over model are compared against test data for a large TPTB with 500

[4] Specific (unit) load in journal bearing = $W/(LD)$, where W is the static load [N], L is the bearing axial length [m], and D the diameter of the bearing [m].

mm in diameter and slenderness ratio L/D = 1. The bearing operates at 3 krpm rotor speed and under 2.5 MPa of specific load. Predictions from the new model are up to 17 ºC closer to the measurements.

The literature review reveals that he lubricant supply flow rate substantially affects both static and dynamic load performance of thrust bearings. Most published computational analyses of starved flow fluid film bearings are specific to journal bearings [1,4], whereas those for thrust bearings are limited to fixed-geometry bearings [3,8].

The work funded by TRC aims to extend the state-of-the-art in this field by building a computational analysis with starved flow and specific to TPTBs.

2. ANALYSIS

2.1 A Thermo-elasto-Hydrodynamic Model for Tiling Pad Thrust Bearing

Figure 3 depicts a schematic view of a TPTB, coordinate systems, and definition of variables. The thickness of the fluid film over pad i^{th} follows from the thrust collar axial location ($e_{C(t)}$), thrust collar misalignment angles (φ, ψ), the pivot axial location ($e_{P(t)}$), elastic deformation of the pad top surface $d_{(r,\theta,t)}$, and the pad tilt angles ($\alpha_{(t)}$,$\beta_{(t)}$). The film thickness equation is,

$$h^i_{(r,\theta,t)} = [e_c - (e^i_P + t_P)] + (\varphi r)\sin\theta - (\psi r)\cos\theta + (\alpha^i r)\sin(\theta^i_P - \theta) + (\beta^i r)\cos(\theta^i_P - \theta) - (\beta^i R^i_P) + d^i_{(r,\theta,t)} \qquad \theta^i_l < \theta < \theta^i_t \tag{1}$$

where t_P is the pad thickness, (θ_l, θ_t) are the circumferential locations of the pad leading edge and the pad trailing edge, respectively, and (R_P, θ_P) denote the pivot location.

The combined solution of a general Reynolds equation [16] and a 3D thermal energy transport equation in the fluid film [17] coupled to a 3D heat conduction equation in the pad [18] delivers the hydrodynamic pressure field $P_{(r,\theta)}$ and the temperature fields for both the fluid film $T_{(r,\theta,z)}$ and the pad $T_{P(r,\theta,z)}$. These equations are,

$$\frac{1}{r}\frac{\partial}{\partial r}\left(rH_r\frac{\partial P}{\partial r}\right)+\frac{1}{r}\frac{\partial}{\partial\theta}\left(H_\theta\frac{1}{r}\frac{\partial P}{\partial\theta}\right)=\Omega\frac{\partial G}{\partial\theta}+\frac{\partial h}{\partial t} \tag{2}$$

$$\rho c_P\left[U\frac{\partial T}{\partial r}+V\frac{\partial T}{r\partial\theta}+W\frac{\partial T}{\partial z}\right]= \kappa\left(1+\frac{Pr}{Pr^*}\frac{\epsilon_m}{\nu}\right)\left[\frac{1}{r}\frac{\partial}{\partial r}\left(r\frac{\partial T}{\partial r}\right)+\frac{1}{r^2}\frac{\partial T^2}{\partial\theta^2}+\frac{\partial T^2}{\partial z^2}\right]+\mu\left(1+\frac{\epsilon_m}{\nu}\right)\left[\left(\frac{\partial U}{\partial z}\right)^2+\left(\frac{\partial V}{\partial z}\right)^2\right] \tag{3}$$

$$\nabla^2\left(T_P\right)=\frac{1}{r}\frac{\partial}{\partial r}\left(r\frac{\partial T_P}{\partial r}\right)+\frac{1}{r^2}\frac{\partial^2 T_P}{\partial\theta^2}+\frac{\partial^2 T_P}{\partial z^2}=0 \tag{4}$$

here H_r, H_θ, and G are turbulent flow functions (see Refs. [16,19]), and Ω is the rotor speed. (ρ, c_P, κ, $\mu_{(T)}$) represent the lubricant density, heat capacity, thermal conductivity, and viscosity, respectively. (U, V, W) denote the components of flow velocity filed in the cylindrical coordinate system. ϵ_m and ϵ_H denote the eddy viscosity for momentum transfer and the eddy viscosity for heat transfer, respectively. Pr is the Prandtl number, and $Pr^* = \epsilon_m/\epsilon_H$ is the turbulent flow Prandtl number with a typical value equal to 0.769 [16].

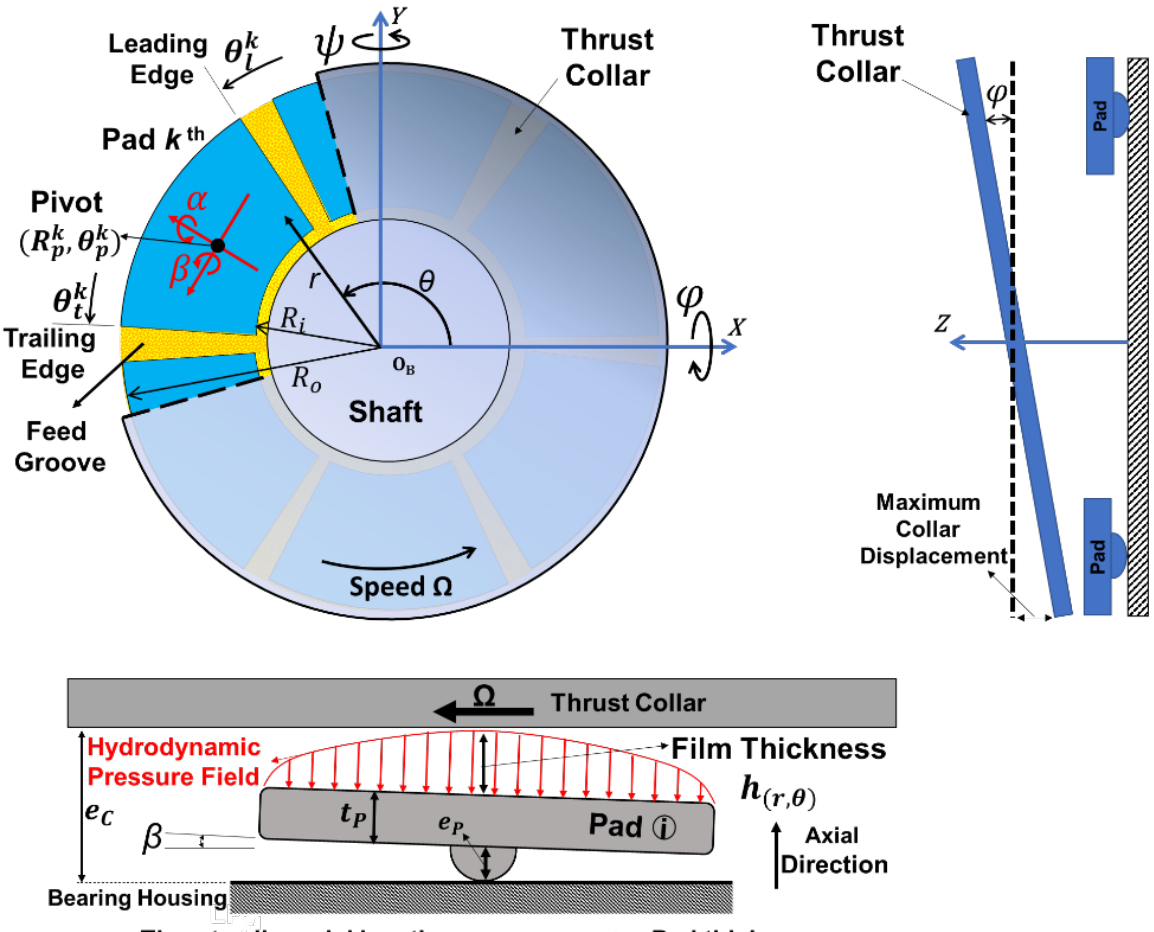

e_c	Thrust collar axial location.	t_P	Pad thickness.
e_P	Pivot thickness.	(X,Y,Z)	Cartesian coordinate system.
O_B	Bearing housing center point.	α, β	Pad radial and circumferential tilt angles.
(r,θ,z)	Global cylindrical coordinate system.	θ_l, θ_t	Leading edge and trailing edge circumferential location.
R_p, θ_p	Pivot radial and circumferential location.	φ, ψ	Misalignment angles of thrust collar around *y* and *x* axes.
R_i, R_o	Pad inner and outer radius.	Ω	Shaft rotational speed

Fig. 2 Schematic views of a TPTB with nomenclature.

A force equilibrium equation, a strain displacement equation, and the material constitutive law govern the elastic deformation of a pad. These equations are [15-16],

$$\mathbf{D}_\sigma^T \boldsymbol{\sigma} + \mathbf{F}_B = 0 \tag{5}$$

$$\varepsilon_{ij} = \frac{1+\nu}{E}\sigma_{ij} - \left(\frac{\nu}{E}\sigma_{kk} + \alpha_T \Delta T_P\right)\delta_{ij} \qquad i, j, k = r, \theta, z \tag{6}$$

$$\boldsymbol{\varepsilon} = \mathbf{D}_u \mathbf{u} \tag{7}$$

where $\mathbf{F}_B$ is an internal body force vector, and $\boldsymbol{\sigma}$ and $\boldsymbol{\varepsilon}$ are the stress and strain vectors, respectively. Parameters E, ν and σ_T represent the pad or liner material elasticity modulus, Poisson ratio, and the thermal expansion coefficient. $\mathbf{D}_\sigma$ and $\mathbf{D}_u$ are gradient operators for the stress and displacement vectors, respectively; see Ref. [20]. A finite element (FE) model discretizes Eqns. (5) to (7) and forms a linear system of algebraic equations for each element,

$$\mathbf{K}^e u = \mathbf{f}_P^e + \mathbf{f}_T^e \tag{8}$$

where $\mathbf{K}^e$ is an element stiffness matrix and $\mathbf{f}_P^e$ and $\mathbf{f}_T^e$ are the load vectors induced by the pressure field acting on the pad top surface and the pad thermal changes, respectively. Next, the FE model assembles all element equations into a global stiffness matrix and a global load vector and enforces the boundary condition at the pivot (spherical or cylindrical). A Cholesky decomposition technique solves the global matrix equation to deliver pad elastic deformations.

Note that flow starvation in a TPTB strongly affects the hydrodynamic pressure field as well as the pad temperature field, both of which produce the pad elastic deformations. Thus accounting for pad elastic deformations is essential for accurate bearing load performance predictions.

To produce predictions for a given operating condition (applied load, rotor speed, supply flow condition); the analysis assumes an initial thrust collar axial location (e_C) and calculates the pressure field $P_{(r,\theta)}$ from Reynolds Eq. (2) and fluid film temperature field $T_{(r,\theta,z)}$ and the pad temperature field $T_{P(r,\theta,z)}$ from Eqns. (3) and (4). Iterations on the pad tilt angles moves the pad into a position where the moment induced by the pressure field around the pivot point is balanced. The FE model of the pad and liner uses the predicted pressure field and pad temperature field to produce elastic deformations for the pad top surface, and updates the fluid film thickness. The analysis repeats until variations of the pressure field is within a convergence criteria of < 0.1%. The integration of the pressure field P over the bearing pads gives the bearing reaction force F_0, though the analysis updates the thrust collar axial location and the analysis repeats until the bearing reaction force balances out against the applied load on the bearing, i.e. $F_{Z_0} + W_{Z_0} = 0$.

At an equilibrium position, a small amplitude period force ($\Delta F e^{i\omega t}$) with frequency ω excites a thrust collar displacement (Δe_C) and pad motions (Δe_P, $\Delta\alpha$, $\Delta\beta$) with identical frequency to produce perturbations in the fluid film thickness and pressure fields. Integration of the perturbed pressure fields over the i^{th} pad generates 16 (=4×4) fluid film complex stiffness coefficients [21],

$$Z_{XY}^{i} = K_{XY}^{i} + i\omega C_{XY}^{i} = \int_{R_i}^{R_o}\int_{\theta_l}^{\theta_T} P_Y^i h_X \, r\,dr\,d\theta; \qquad X, Y = e_C, e_P, \alpha, \beta \tag{9}$$

where **K** and **C** are matrices of the film stiffness and damping coefficients, respectively, and,

$$\left[h_{e_C} \;\; h_{e_P} \;\; h_\alpha \;\; h_\beta\right] = \left[1 \quad -1 \quad r\sin\left(\theta_P - \theta\right) \quad r\cos\left(\theta_P - \theta\right) - R_P\right] \tag{10}$$

A frequency reduced model [21] assumes all pads move with the same frequency (ω) to reduce the $16\times N_{\text{Pad}}$ stiffness coefficients into axial stiffness and damping coefficients (K_z, C_z).

2.2 A Flow Thermal Mixing Model in the Bearing Grooves

A conservative thermal energy equation balances the heat flowing inside and outside of a feed groove to determine the temperature of the flow entering the leading edge of the downstream pad. Figure 3 shows a schematic view of the flow streaming into and out of a feed groove in a TPTB. A groove receives a hot stream of flow ($Q_{TE}^{i-1}, T_{TE}^{i-1}$) from the upstream pad and a cold supply flow (Q_{Su}^{i}, T_{Su}). In case of a flooded lubrication method (not evacuated), previous work in Ref. [5,9,10] show the oil churning at a bearing ID also flows into a feed ($Q_{ID}^{i-1}, T_{ID}^{i-1}$). The oil departs the groove to enter the downstream pad leading edge and while any additional flow is pushed to the bearing OD as a side leakage. Further, a feed groove may also experience a back flow (Q_{BF}^{i}, T_{BF}^{i}) from the downstream pad where the oil is pushed back into the groove due to a large pressure gradient at the pad leading edge. Accordingly, for bearings with end seals, the temperature at a pad leading edge is

$$T_{LE}^{i-1} = \frac{Q_{Su}^{i} T_{Su} + Q_{TE}^{i-1} T_{TE}^{i-1} + Q_{ID}^{i-1} T_{ID}^{i-1} + Q_{BF}^{i} T_{BF}^{i}}{Q_{LE}^{i} + Q_{SL}^{i}} \tag{11}$$

where,

$$Q_{SL}^{i} = Q_{Su}^{i} + Q_{TE}^{i-1} + Q_{ID}^{i-1} + Q_{BF}^{i} - Q_{LE}^{i} \tag{12}$$

For bearings with evacuated ends, the flow exiting a pad at both the ID and OD leaves the bearing housing to return to sump. Hence, the inlet flow temperature becomes,

$$T_{LE}^{i-1} = \frac{Q_{Su}^{i} T_{Su} + Q_{TE}^{i-1} T_{TE}^{i-1} + Q_{BF}^{i} T_{BF}^{i}}{Q_{LE}^{i} + Q_{SL}^{i}} \tag{13}$$

where,

$$Q_{SL}^{i} = Q_{Su}^{i} + Q_{TE}^{i-1} + Q_{BF}^{i} - Q_{LE}^{i} \tag{14}$$

Note based on the (simple) thermal energy balance Eqn. (11), the pad inlet flow temperature is a function of the supply flow rate $\left(Q_{Su}^{i}\right)$, i.e., an increase in supply flow rate results in a lower pad inlet temperature. In Ref. [9], Glavatskih et al. uses an identical thermal energy balance eqn. and further validates the model predictions of film thickness, pad temperature rise and drag power loss vs. measurements for a six-pad TPTB operating under specific load per pad = 0.5- 2.0 MPa and at rotor speed = 1.5-3.0 krpm.

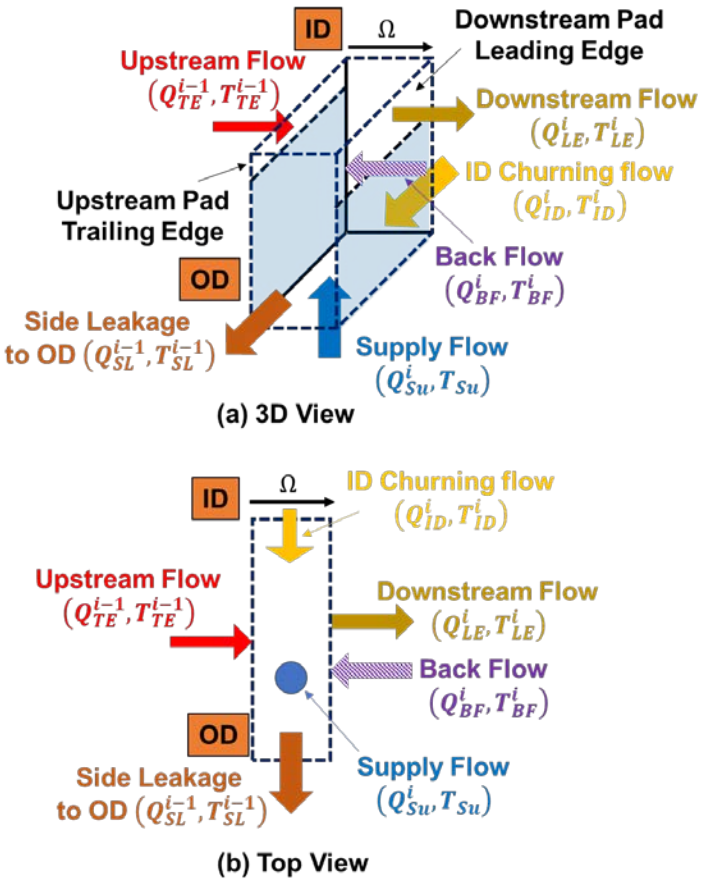

Fig. 3: Schematic view of the flows moving into and out of a feed groove in a TPTB.

2.3 A Flow Starvation - Over-Flooded Model for Tilting Pad Thrust Bearings

The work here implements the flow starvation model by San Andrés et al. [1] to quantify the effect of flow rate on the performance of TPTBs. In a flooded flow condition, the supply flow rate must be enough to fully fill in the gap region between the thrust collar and bearing pads. Any additional flow is quickly forced out through the bearing OD and which produces churning power loss if the bearing is not evacuated, i.e. end seals on the shaft trap the oil inside the bearing housing.

If the supply flow is less than the one needed, the bearing starves. Figure 3 portrays a schematic view of a bearing pad operating under flow starvation. Q_{TE}^{i-1} is the (fraction of) flow leaving an upstream pad that is carried by the rotating collar, while Q_{Su}^{i} is the externally supplied flow that is not enough to fill in the gap at the pad leading edge. The mixing of both flows occurs at a distance inside the pad. The arc length defined as effective is the region where a hydrodynamic pressure builds to sustain an applied load. A flow starved pad has a shorter effective arc length than the actual physical length of a pad resulting in a smaller effective pivot offset for the lubricated part of the pad.

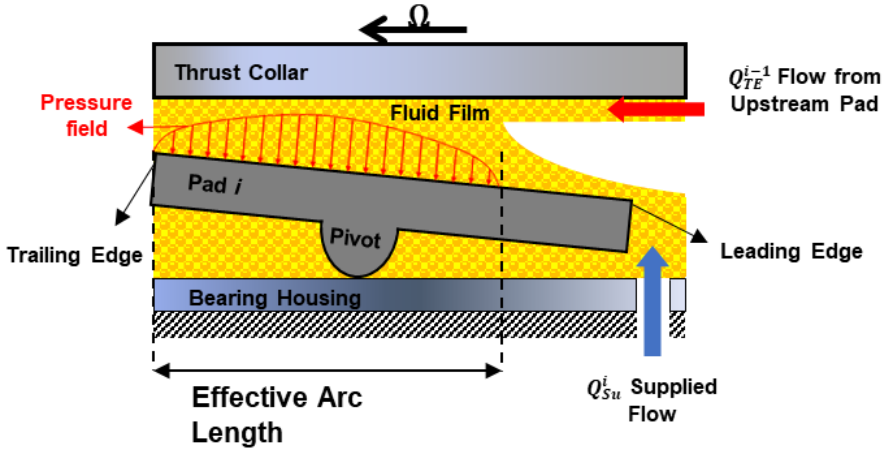

Fig. 4: Idealized view of a flow starvation in a pad. Q_{Su} and Q_{TE} are the (cold) supply flow and the (hot) flow from an upstream pad.

During the solution process, the analysis initially predicts the bearing performance by first considering pressure boundary conditions (not flow) to determine the nominal (demand or supply) flow rate, the one needed to wet all the pads in a whole bearing. Over flooded operation ensues when the actual supply flow rate exceeds the nominal flow; and here the analysis assumes the extra flow simply displaces toward the bearing OD to return to sump flow. Note an increase in supply flow rate lowers the pad inlet flow temperature while the groove side leakage increases, see the

thermal energy balance Eqns. in a feed groove (Eqn.(11) for sealed ends and Eqn. (13) for evacuated ends bearings).

On the other hand, a starved flow condition ensues when the actual supply flow rate is lesser than the nominal. Here the analysis iteratively reduces the film arc length until the supply flow rate is enough to fully fill the film gap i.e.,

$$Q^i_{SL} = 0 \quad \text{and} \quad Q^i_{LE} = Q^i_{Su} + Q^{i-1}_{TE} + Q^{i-1}_{ID} + Q^i_{BF} \tag{15}$$

Note when a groove side leakage flow is null, all the heat carried into the groove from the upstream pad flows to the inlet of the downstream pad, see the thermal energy balance at a groove, Eqns. (11) and (13).

Ideally all feed grooves in a thrust bearing receive an equal apportion of the supplied flow rate. However, a static misalignment between the thrust collar and the bearing pads and housing imposes distinct flow conditions on each lubricant feed groove.

Figure 5 shows idealized views of the (local network) flow distribution through holes into a thrust bearing operating with either a perfectly aligned thrust collar or with a misaligned thrust collar ($\phi > 0$). The misalignment causes pads 1 to 3 to open their leading edges thus requiring of more flow. The exact opposite occurs for pads 4 to 6 that operate with smaller film thicknesses and demand lesser flow rates.

In lubrication, the local circumferential flow rate through a small gap (film) adds the flow dragged by the surface speed (Couette flow) to the flow induced by a gradient of the pressure field (Poiseuille flow). Since the hydrodynamic pressure field has a maximum inside the pad, it stands to reason that the Poiseuille flow is opposite to the direction of collar rotation in a region near a leading edge of a pad. At the trailing edge of a pad, the pressure driven flow is in the same direction as the surface speed. Clearly the flows leaving a pad through its inner and outer radii are pressure induced.

Abdollahi and San Andrés [4] define C_i an indicator for the demand of supply flow for an i_{th} pad as the ratio of Couette flow (shear driven) entering the leading edge of a downstream pad ($Q^i_{Couette}\big|_{\theta=\theta_{LE}}$) over the sum of the overall flow $\left(Q^{i-1}_{Couette}\big|_{\theta=\theta_{TE}} + Q^{i-1}_{Poiseuille}\big|_{\theta=\theta_{TE}}\right)$ leaving the upstream pad and the Poiseuille flow $\left|Q^i_{Poiseuille}\big|_{\theta=\theta_{LE}}\right|$ exiting through the pad leading edge. That is, [4]

$$C^i = \frac{Q^i_{Couette}\Big|_{\theta=\theta_{LE}}}{\left|Q^i_{Poiseuille}\Big|_{\theta=\theta_{LE}}\right| + \left(Q^{i-1}_{Couette}\Big|_{\theta=\theta_{TE}} + Q^{i-1}_{Poiseuille}\Big|_{\theta=\theta_{TE}}\right)} \quad i=1,2,\ldots N_{pad} \tag{16}$$

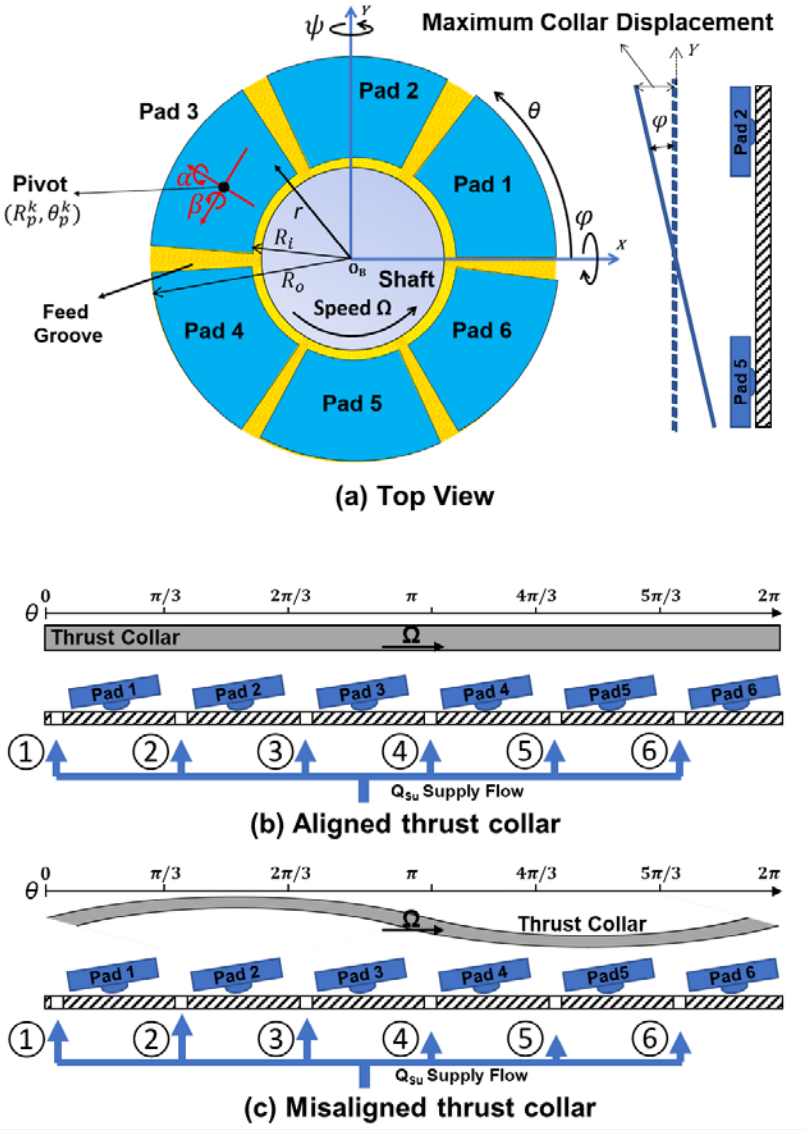

Fig. 5: Idealized views of supply flow distribution through holes in a TPTB with aligned and misaligned thrust collars.

The Couette flow at angle θ and through the pad width (R_o - R_i) is,

$$Q_{Couette} = \int_{R_i}^{R_o} \frac{r\Omega \int_0^{h_{(r,\theta)}} \int_0^z \xi_4(\hat{z})\,d\hat{z}}{\int_0^{h_{(r,\theta)}} \xi_4(z)}\,drdz \tag{17}$$

whereas the Poiseuille flow equals

$$Q_{Poiseuille} = \int_{R_i}^{R_o} \frac{1}{r}\frac{\partial P}{\partial \theta}\left[\frac{\int_0^{h_{(r,\theta)}} \xi_1(z)\, dz}{\int_0^{h_{(r,\theta)}} \xi_2(z)\, dz} \int_0^{h_{(r,\theta)}} \int_0^{z} \xi_1(\hat{z})\, d\hat{z}\, dz - \int_0^{h_{(r,\theta)}} \int_0^{z} \xi_1(\hat{z})\, d\hat{z}\, dz\right] dr \tag{18}$$

where ξ_1 to ξ_4 are turbulence flow functions, see Ref. [16]. Note the demand factor C^i for a fluid with viscosity μ is,

$$C^i = \frac{\frac{\Omega}{2}\int_{R_i}^{R_o} r h^i_{(r,\theta_{LE})}\, dr}{\int_{R_i}^{R_o} \frac{\left(h^i_{(r,\theta_{LE})}\right)^3}{12\mu}\frac{\partial P^i}{r\partial\theta}\, dr + \left(\frac{\Omega}{2}\int_{R_i}^{R_o} r h^{i-1}_{(r,\theta_{TE})}\, dr - \int_{R_i}^{R_o} \frac{\left(h^{i-1}_{(r,\theta_{TE})}\right)^3}{12\mu}\frac{\partial P^{i-1}}{r\partial\theta}\, dr\right)} \tag{19}$$

Borrowed from Henry et al. [22] an example eight-pad fixed-geometry TB with ID = 50 mm, OD = 90 mm and 38˚ in pad arc length[1], Figure 6 shows the predicted C^i vs (a) thrust collar misalignment, (b) rotor speed, and (c) specific load per pad. The misalignment angle equals the maximum collar axial displacement Δz [μm] divided by inner radius R_o [mm]. Expectedly $C^i = 1/N_{\text{pad}} = 0.125$ for operation with a perfectly aligned thrust color. In Figure 6(a), as the bearing operates at 10 krpm of rotor speed and under an average specific load of 3 MPa/pad, C_i for each pad shows a significant linear variation (min 0.10 to max 0.16) as the misalignment increases. In Figure 6(b), the rotor speed ranges from 2 krpm to 10 krpm while the bearing operates under an average 3 MPa specific load/pad and with a large, 0.4 μm/mm, thrust collar misalignment. Each pad has a distinct C^i on account of the misalignment but its variation with shaft speed does not exceed 9% with respect to predicted magnitude for the top speed condition. In Figure 6(c), the rotor speed = 10 krpm and the collar misalignment = 0.4 μm/mm while the average load per pad increases from 0.2 MPa to 3 MPa. Note Ci also shows a substantial dependency on the applied load.

[1] The oil is ISO VG46 with a viscosity of 41mPa.s at 40 °C, a density of 856 kg/m^3, and 2.01 kJ/(kg˚C) in heat capacity [22].

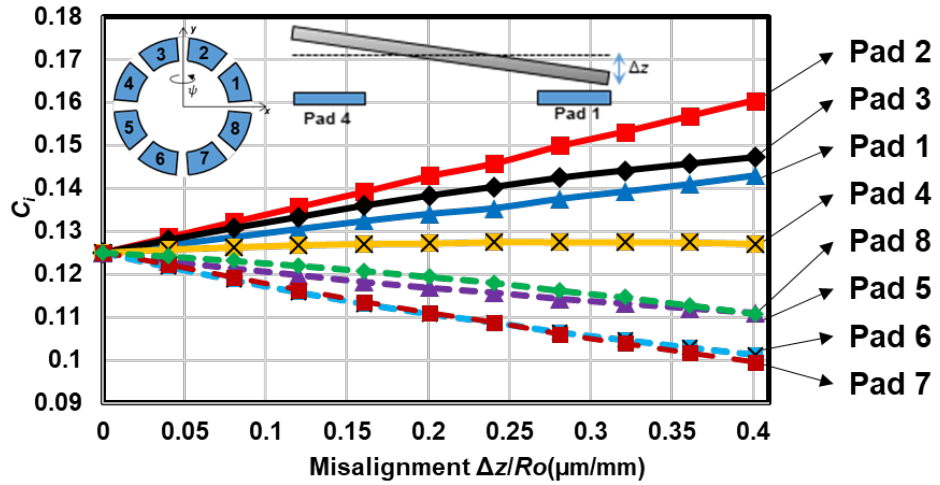

(a) Speed = 4 krpm and Load = 3 MPa/pad

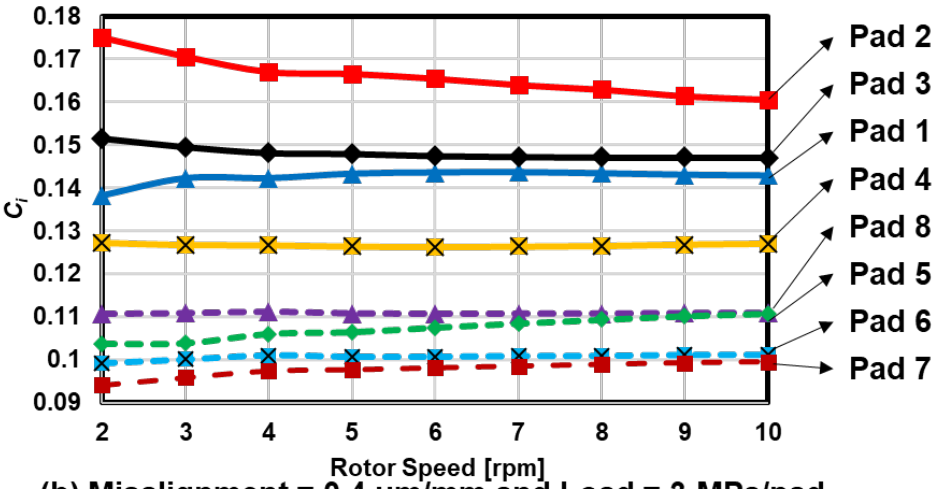

(b) Misalignment = 0.4 μm/mm and Load = 3 MPa/pad

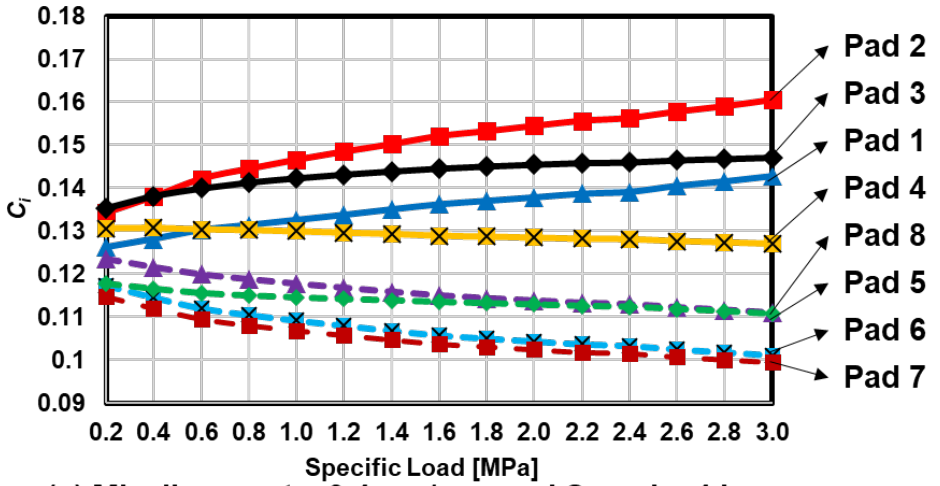

(c) Misalignment = 0.4 μm/mm and Speed = 4 krpm

Fig. 6: Predicted supply flow share for each pad in a fixed-geometry TB vs (a) thrust collar static misalignment, (b) rotor speed, and (c) specific load per pad.

3. RESULTS AND DISCUSSION

Effect of Flow Reduction on the Performance of a TPTB

Mikula [23] and Capitao et al. [7] measure pad subsurface temperature rises and oil exit temperature rise in a centrally pivoted tilting pad thrust bearing (TPTB) operating under three supply flow rates: the manufacturer recommended flow rate, 50% higher and 50% lesser than recommended rate.

This work uses the configuration of the test TPTB in Refs. [23, 7] to evaluate the effect of supply flow rate on the TB load performance. Table 1 highlights the bearing configuration, lubricant properties, and operating conditions. The bearing has eight pads with ID=133 mm, OD=267 mm and 38° pad arc length. The bearing operates at 4 krpm ($R_o\Omega$ = 54m/s) and 10 krpm ($R_o\Omega$ = 135m/s) and under a specific load/pad ranging from 0.7 MPa to 3.5 MPa.

Figure 7 depicts the supply flow rate recommended by the bearing manufacturer and predicted nominal flow rate for operation at 4 krpm and 10 krpm vs specific load per pad [23]. Note, opposed to the recommended flow rate, the predicted nominal flow rate required to fully fill the pads' films decreases from 34 LPM to 10 LPM at 4 krpm, and from 58 LPM to 38 LPM at 10 krpm as the specific load increases from 0.7 MPa/pad to 3.4 MPa/pad. **The marked differences (magnitude and trend) point out to an oversight in the flow prediction.**

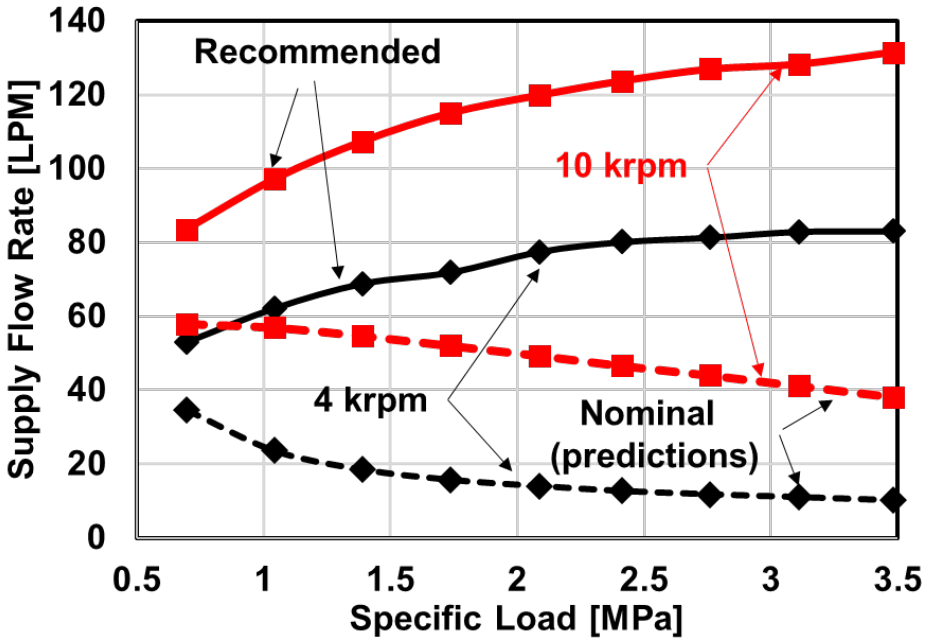

Fig. 7: Recommended and predicted (nominal) supply flow rate vs. specific load/pas for TPTB in Refs. [23, 7].

Table 1: Geometry and operating conditions for example TPTB in Refs. [23, 7].

Bearing Properties			
Number of pads, N_P		8	
Inner diameter, *ID*		133	mm
Outer diameter, *OD*		267	mm
Pad arc length		38	°
Pivot radial offset		50	%
Pivot circumferential offset		50	%
Pad thickness*, t_p		20	mm
Babbitt thickness*		2.0	mm
Pad Area		45.6	cm^2
Operating Condition			
Specific load per pad		0.7-3.5	MPa
Shaft rotational speed		4-10	krpm
Supply pressure*		1.4	bar
Fluid Properties		**ISO VG32**	
Viscosity-temperature coefficient*		0.0247	1/˚C
Viscosity (at 46 ˚C)		22	cPoise
Density		821	kg/m^3
Specific heat capacity		2.17	kJ/(kg˚C)
Thermal conductivity coefficient		0.13	W/(m˚C)
Pad Material Properties**	**Steel**	**Babbitt**	
Conductivity	50	55	W/(m ˚C)
Elasticity module	210	52	GPa
Thermal expansion	12×10^{-6}	23×10^{-6}	1/ ˚C
Poisson ratio	0.3	0.3	-
Thermal Properties			
Finite Element reference temperature**		20	˚C
Heat transfer coefficient on back of pad**		100	$W/(m^2$ ˚C)

* Assumed or calculated based on the available data.
** Taken from Ref. [24].

In prior work [25], the authors validate their model with comparisons of predicted pad subsurface temperature rise vs. test data recorded under a fully flooded condition, the comparisons covered a wide range of rotor speeds from laminar flow at 4 krpm to fully turbulent flow at 13 krpm. To validate the current model against measurements in Refs. [7, 23], the following results benchmark predictions for the pads' subsurface (0.8 mm below the Babbit surface) temperature rise and the exit or discharge oil temperature rise at specific supplied flow rates.

Figure 8 depict the predicted exit oil temperature rise and temperature rise at the pad mid radius and angular locations denoting a pad leading edge, pad center, and pad trailing edge from the present analysis. The experimental data in Ref. [23] relates to operation at three distinct supply

flow rates; 50%, 100% and 150% of recommended flow. The bearing operates at 4 krpm angular speed and under a specific load per pad ranging from 0.7 MPa to 3.4 MPa. The flow is laminar for the operating conditions noted.

In Figure 8 (a), the experimentally recorded oil exit temperature rise does not vary with an increasing load and increases significantly as the flow rate reduces to 50% of recommended rate. Operation with an over flow (150%) reduces the oil exit temperature. The difference between oil exit temperatures for the 50% and 150% flows is sizable. Predictions for the exit temperature rise agree with the measurements, in particular for the flooded and over-flooded conditions. In any case, the maximum difference between a prediction and the test magnitude is ~ 4 °C.

In Figure 8 (b-d), the measured pad subsurface temperatures increase almost linearly with the specific load while showing a minor dependency on the supplied flow, above or below the recommended rate. The difference in temperatures at the pad trailing edge (hotter) and at the pad leading edge (colder) increases with the specific load. The predictions of temperature are very accurate when compared to those measured temperature at the pad center and at its trailing edge. The predicted temperature at the pad leading edge is higher than the one measured for operation with flow starvation. The discrepancy between measurements and predictions does not exceed 11 °C (14% with respect to measurements). Note a 50% supply flow rate is still large enough to fill the gap between the bearing pads and the thrust collar as there is no reduction in the pads effective length. Likely this is because the film thickness over the wetted area also decreases as the supply flow rate decreases.

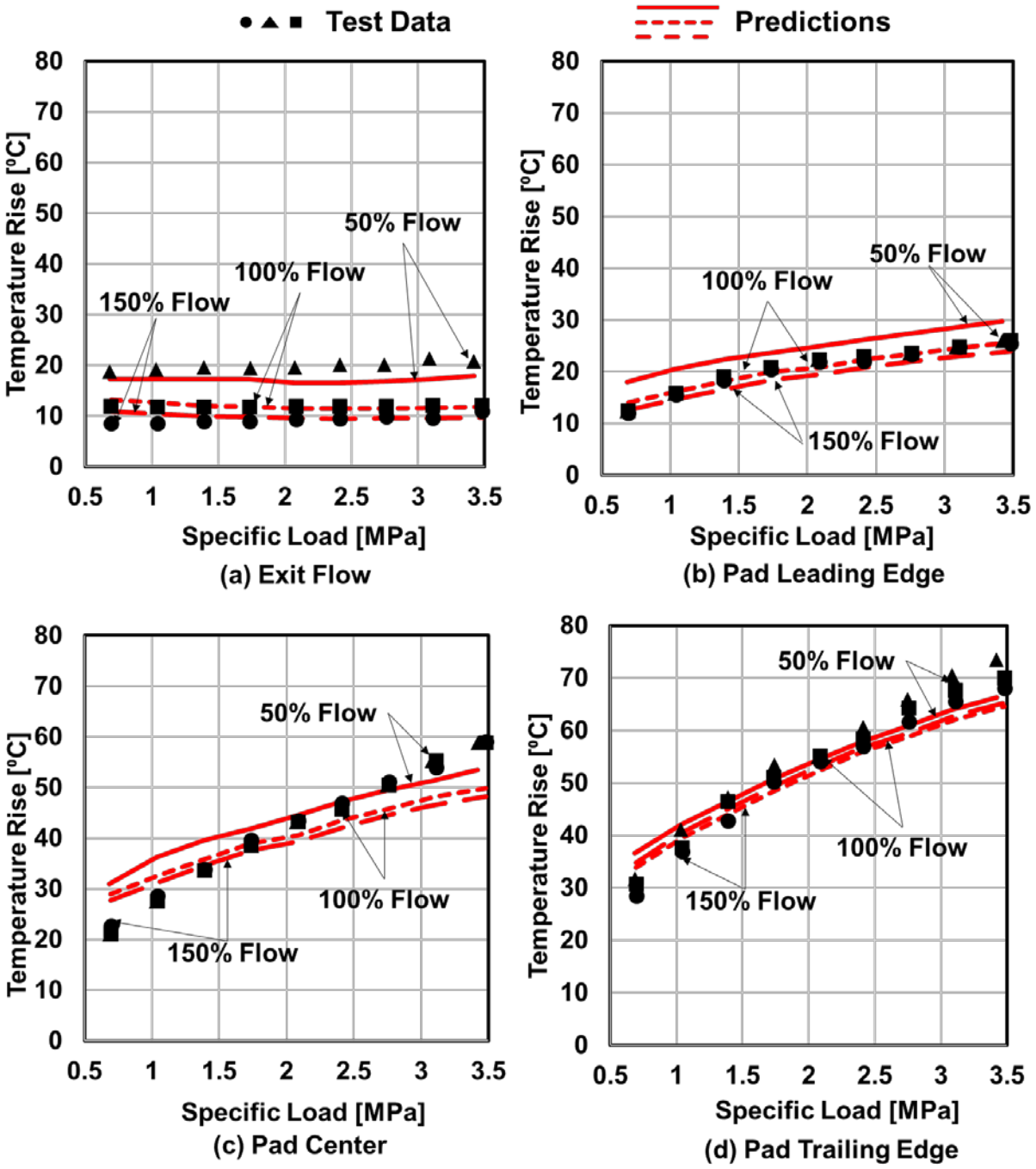

Fig. 8: Predicted (a) oil exit temperature rise and subsurface temperature rises in (b) pad leading edge, (c) pad center and (c) pad trailing edge. Test data for a TPTB supplied with 50%, 100%, and 150% of nominal flow rate [23]. Supply temperature = 46°C and shaft speed = 4 krpm.

For operation at 10 krpm rotor speed and with the fluid flow as fully turbulent, Figure 9 shows predictions and test data for the oil exit temperature rise and pad subsurface temperature rise at an location at a 75% offset from the pad leading edge and 75% way from the pad inner radius. Note

the oil exit temperature slightly decreases with applied load and is much higher for the starved flow condition, the prediction lagging the recorded magnitude by nearly 10 °C, Operation with an over flow (1.5 of recommended rate) produces a drop in the oil exit temperature albeit increasing as the applied load increases. The predictions on the other hand do not show the apparent cooling effect as the load increases.

The measured pad subsurface temperature rise shows a linear increase with specific load. Under a light load of 0.7 MPa/pad, the pad temperature rise increases by 42%, from 43 °C to 61°C, as the supply flow decreases to 50% of the recommended rate. The largest increase in pad temperature equals 90 °C and is independent of the flow condition, starved or over flooded. Considering the oil supply temperature is 46 °C, a pad temperature of 136 °C is just above the Babbitt critical temperature of 130 °C. Experiments in Guo et al. [26] show that operation with a pad temperature exceeding 130 °C damages the Babbitt and results in bearing failure. The predicted pad temperature rise shows a trend consistent with the reduction in flow rate and is also proportional to the applied load. The differences with the measured temperatures decreases as the load increases.

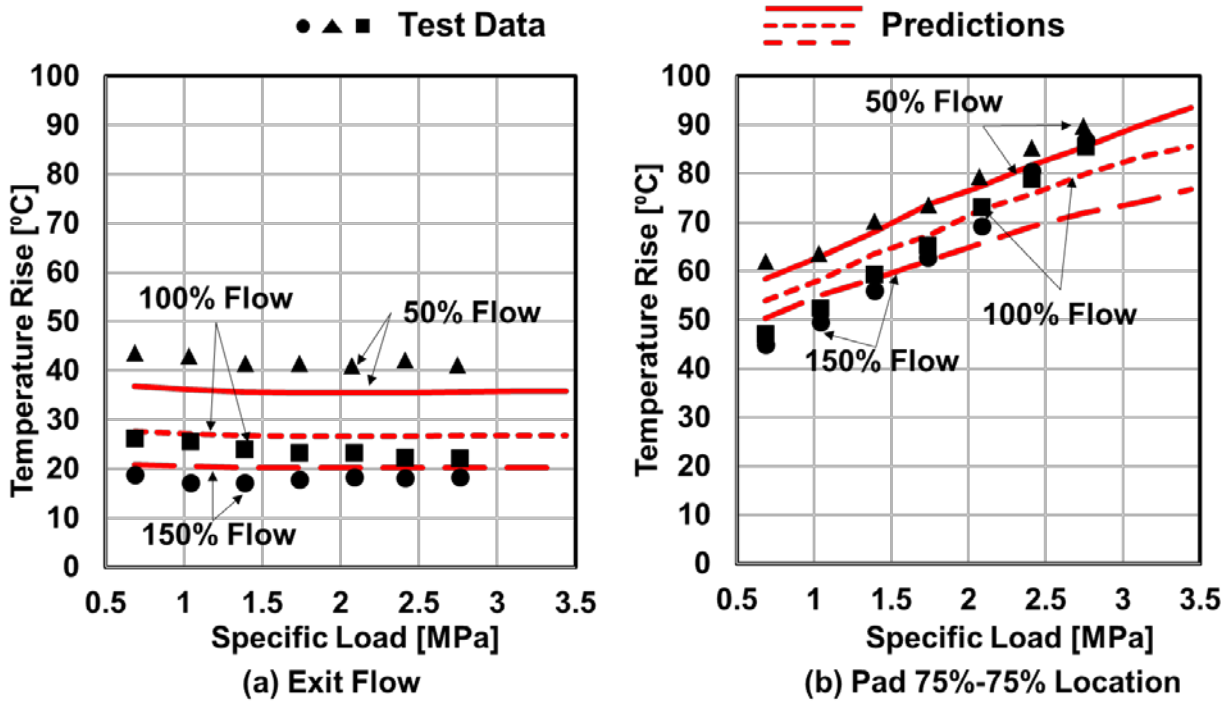

Fig. 9: Predicted (a) oil exit temperature rise and (b) pad subsurface temperature rise at 75% offset from pad leading edge and 75% offset from pad inner radius. Test data for a TPTB supplied with 50%, 100%, and 150% of nominal flow rate [7]. Supply temperature = 46°C and shaft speed = 4 krpm.

For the example TPTB, Figure 10 showcases on the left and right graphs the predicted fluid film thickness and hydrodynamic pressure fields, respectively, for oil flow supply conditions with a nominal rate = 23 LPM (top), 60% nominal flow (middle), and 30% nominal flow (bottom). The rotor speed is 4 krpm and the specific load per pad is 1 MPa. Note the bearing ends are assumed to be evacuated (no end seals) meaning the oil that exits the pad, at its OD and ID, also leaves the bearing. Note for a flooded lubrication method with end seals, the oil leaving the pad at its ID remains in the groove oil bath and would be considered as carrying energy for the groove thermal energy balance, Eqn. (11).

In Figure 10 (a) for a fully flooded flow condition, the minimum film thickness varies from a maximum of 73 μm at the corner of the pad leading edge and OD to a minimum of 33 μm at the pad trailing edge and ID The hydrodynamic pressure has a peak of 2.5 MPa near the pad center and gradually drops toward ambient at the pad edges. In Figure 10 (b) for a 60% nominal flow, the minimum film thickness field decreases roughly by 19 μm (42% lesser than for flooded condition) while the maximum thickness equals 58 μm. The peak hydrodynamic pressure, however, increases by 36% to 3.4 MPa. In Figure 10 (c) for a lesser flow at 30% nominal, the smallest film thickness is 11 μm (1/3 of gap for flooded) while the peak pressure nearly doubles to reach 4.7 MPa. Note the labels in the pressure graphs indicating portions of the pad region that are denuded (starved) of lubricant, i.e., these regions contain air.

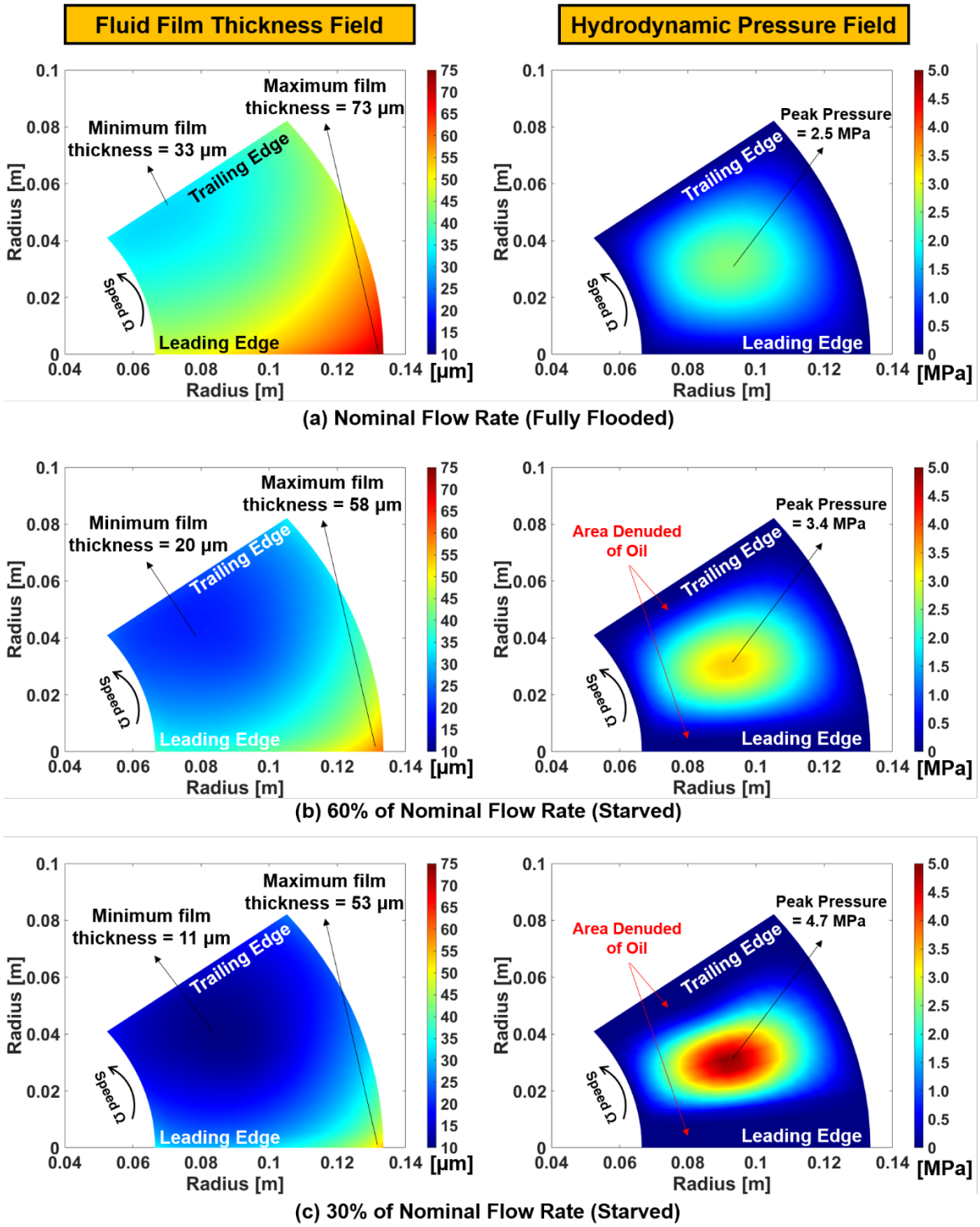

Fig. 10: Predicted film thickness field (left) and hydrodynamic pressure filed (right) for a TPTB operating with (a) nominal flow and with a starved flow at (b) 60% and (c) 30% of nominal rate. Supply temperature = 46 ºC, specific load = 1 MPa/pad, rotor speed = 4 krpm.

For the same operating conditions as those in Fig. 10, Figure 11 shows the pressure profile (top graph) and film thickness at the pad mid radius arc. The differences in pressure profile are marked

as the flow rate decreases. In short, when the pad starves of lubricant, the film thickness decreases and the hydrodynamic pressure region narrows and *bulges* toward the middle of the pad. The pad wetted arc extent lessens, as expected. Note the pad minimum film thickness moves toward the pad center as the supplied flow decreases to make a diverging gap at the pad trailing edge.

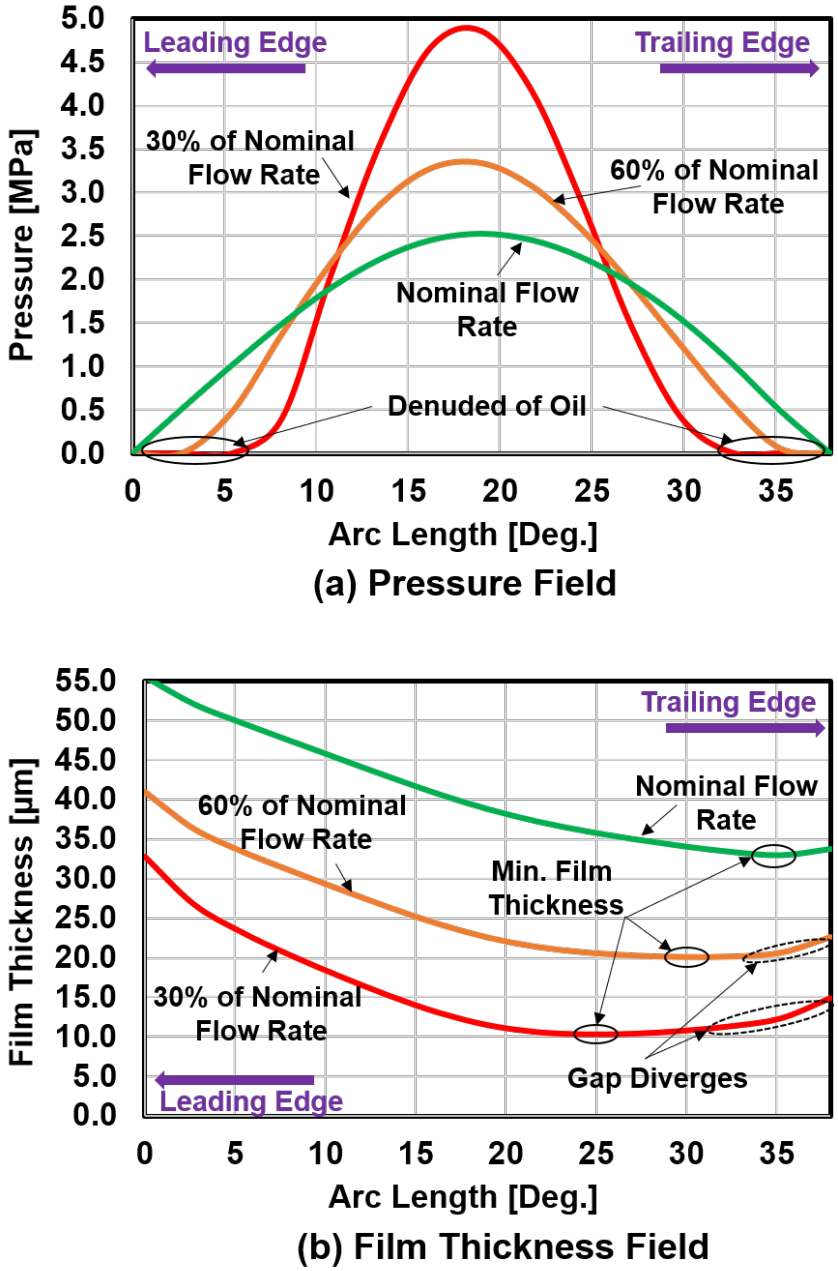

Fig. 11: Predicted (a) pressure field and (b) film thickness field at pad mid radius vs. angle θ. TPTB operating with nominal flow rate and under starvation with 60% and 30% of nominal flow rate. Supply temperature = 46 ºC, specific load = 1 MPa/pad, rotor speed = 4 krpm.

Figure 12 portrays the pad temperature field (left graphs) and the pad thermal deformation field (right graphs) as the supply flow rate decreases (top to bottom). Recall the oil supply temperature is 46 ^{o}C. Under a nominal flow condition see Fig. 12(a), the pad temperature field increases from 62 °C at the bottom surface of the pad leading edge to a maximum of 109 °C at the Babbitt top surface near the pad trailing edge. Accordingly, the pad thermal deformation shows crowning with a peak of 16 μm at its center. A reduction in supply flow to 60% of nominal, see Fig. 12(b), produces a 22 °C (20%) increase in the pad peak temperature followed by a 44% increase in thermal deformation to a peak of 23 μm. As the supply flow rate further decreases to just 30% of nominal, see Fig. 12(c), the pad peak temperature reaches 156 °C, a 43% increase compared to that obtained with a nominal flow rate, and well above the Babbitt material critical temperature of 130 ^{o}C. The pad peak thermal deformation also almost doubles to 30 μm.

Note the predicted pad mechanical deformations (not shown here) are relatively insignificant (maximum of 1 μm) whereas thermal deformations dominate the pads overall deformation. Nonetheless, the predicted pad mechanical deformation decreases under a starved flow condition as the pressure field concentrates more over the pad center area supported by the pivot.

The following figures depict various TPTB performance parameters versus supply flow rate varying over a wide range, 25% to 150% nominal, for operation with shaft speed at 4 krpm and under three specific loads/pad, 1 to 3 MPa. Figure 13 shows the predicted (a) minimum film thickness, (b) peak hydrodynamic pressure, and (c) bearing drag torque vs. flow rate. Note that operation with an over flow (> 100%) affects little the peak pressure and the minimum film thickness but does increase the drag torque (and power). On the other hand, under starved flow conditions, the minimum film thickness substantially drops linearly with a reduction in flow to reach a too low (critical) magnitude, 8 μm [27] or lesser for the largest load applied. Similarly, the peak pressure increases up to 2.5 times as the supply flow rate decreases. Measurements in Ref. [28] shows the ultimate strength of white-metal (Babbitt) significantly lowers at high temperatures and could be as low as 18 MPa. The predicted pad peak pressure remains mostly below the Babbitt ultimate strength except for operation with a 3 MPa/pad and a supply flow rate lesser than 30% nominal. In Figure 13(c), the predicted drag torque decreases almost linearly as the supplied flow rate decreases. For instance, the drag torque for operating under a 3 MPa specific load per pad drops roughly by half from 38 N.m to 20 N.m as the supply flow rate decreases from 150% to 25% of the nominal rate.

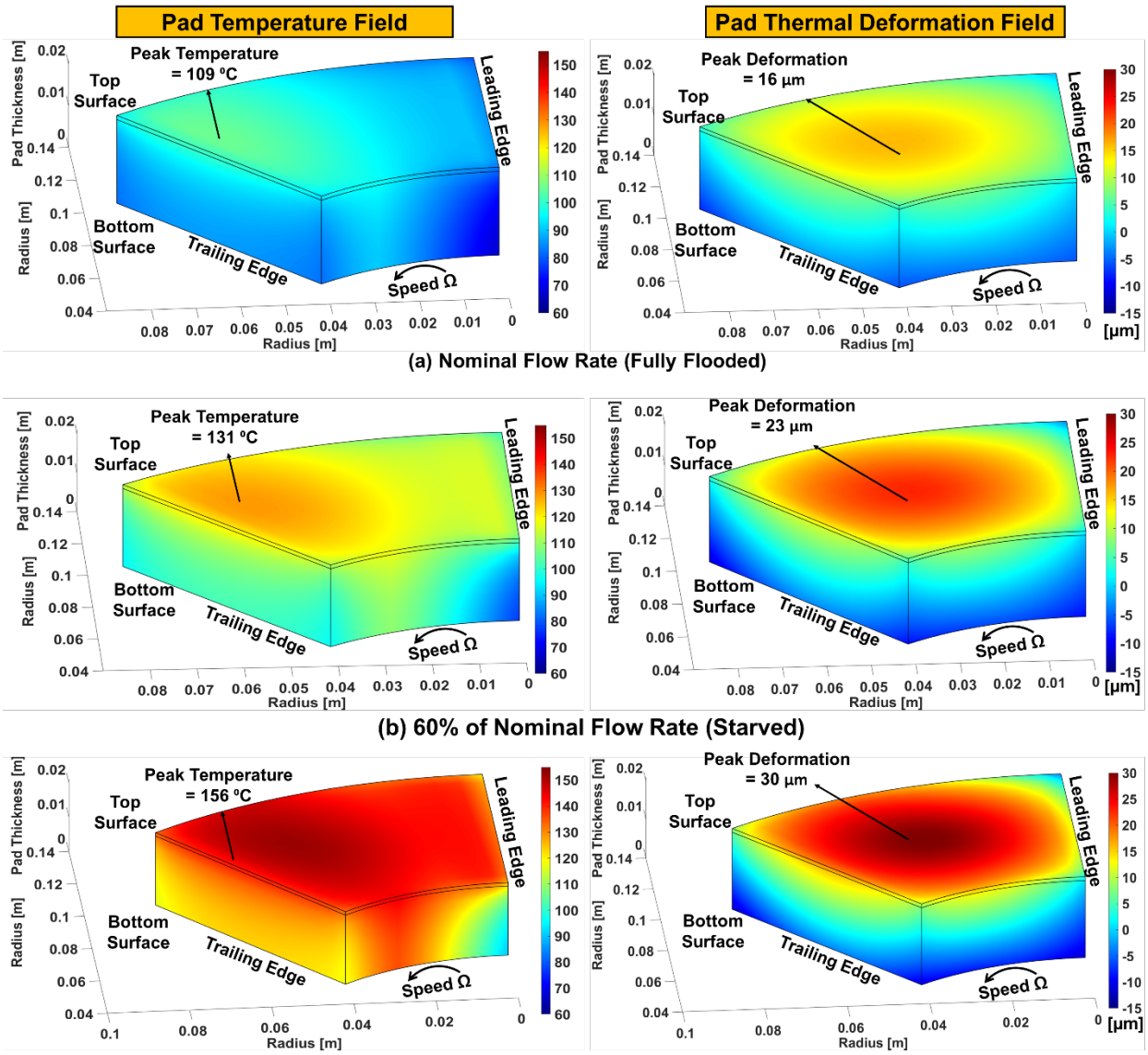

Fig. 12: Predicted pad temperature field (left) and thermally induced pad deformation field (right). TPTB operating with nominal flow rate and under starvation with 60% and 30% of nominal flow rate. Supply temperature = 46 ºC, specific load = 1 MPa/pad, rotor speed = 4 krpm.

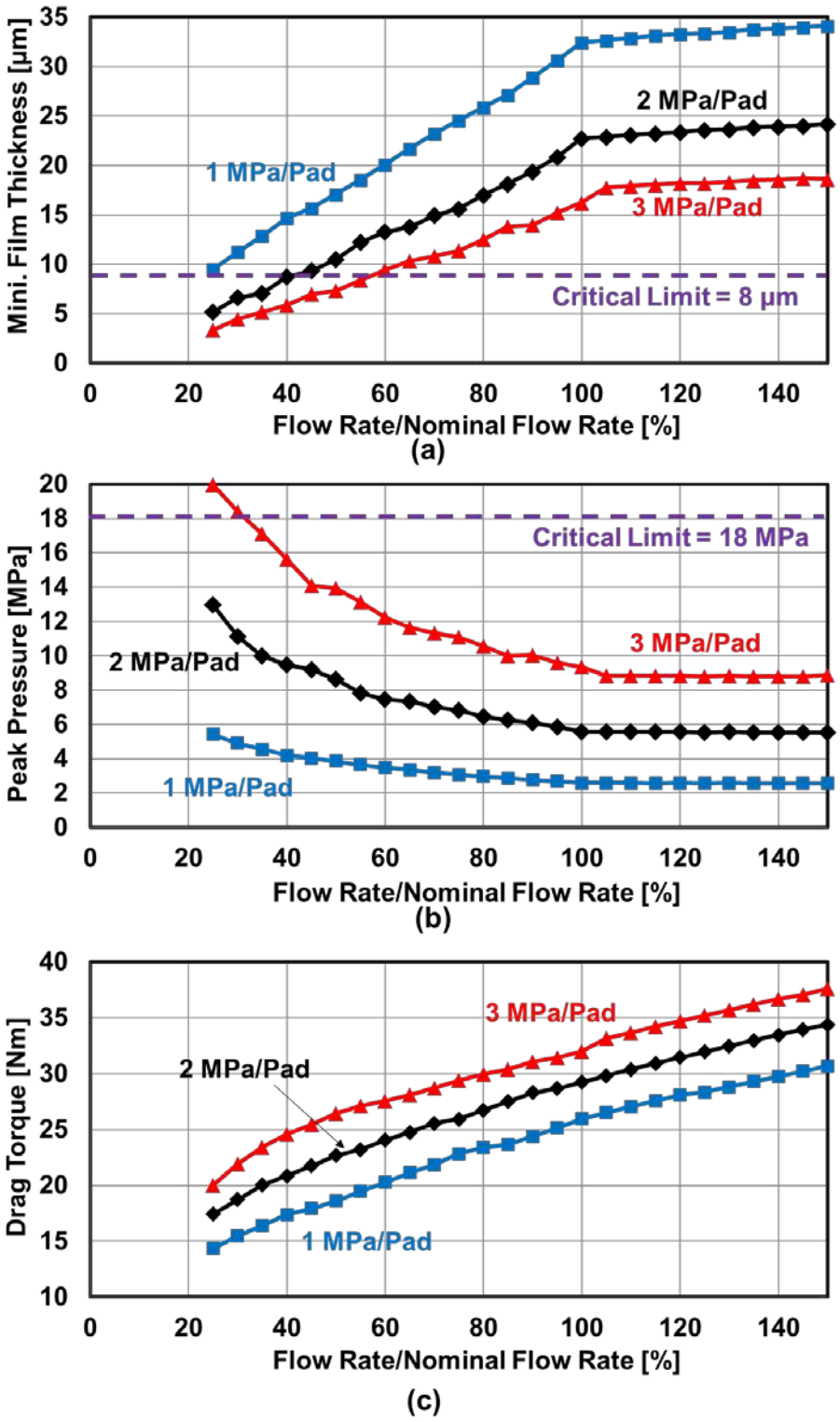

Fig. 13: Predicted (a) minimum film thickness, (b) peak pressure, and (c) bearing drag torque vs flow rate and specific load/pad: 1 MPa, 2 MPa, and 3 MPa. Supply temperature = 46 ºC, rotor speed = 4 krpm.

Figure 14 depicts the peak temperature rise and thermal deformation in a pad vs supply flow and three applied loads, 1 to 3 MPa/pad. (From Fig. 11) Note the peak temperature occurs at the Babbitt top surface - trailing edge and OD, whereas the peak material deformation happens at the center of the pad. In an agreement with measurements in Refs. [2, 7], the predicted pad temperature raise is insignificant with an increase in supply flow rate above nominal, whereas a flow reduction below the nominal rate produces a substantial temperature raise. The predicted pad peak deformation also linearly increase as the supplied flow decreases below nominal. Recall that the Babbitt critical temperature = 130°C, With a 3 MPa/pad, the peak temperature nearly doubles from 76 °C to 133 °C as the supply flow rate reduces from nominal to just 25% flow. Note the fluid film peak temperature rise (not shown here) is slightly larger than the pad peak temperature and close to 180 °C, near the oil flash point of 196°C for ISO VG32 oil.

Lastly, Figure 15 shows the predicted bearing (synchronous speed) axial stiffness coefficient (K_z), damping coefficient (C_z), and ratio ($\Omega C_z / K_z$) vs supply flow. An over flooded flow condition has no effect on the force coefficients. As the bearing starves of flow, the bearing axial stiffness coefficient increases while the axial damping coefficient drops. For operating under a heavy load of 3 MPa/pad, K_z triples, from 9 GN/m to 28 GN/m, as the supply flow rate decreases from nominal to 25%, whereas C_z decreases by 30% =, from 8.1 MN.s/m to 5.6 MN.s/m. Note as the supply flow rate decreases, the ratio ($\Omega C_z/K_z$) linearly drops, in particular under a light load, to reveal the absence of (axial) damping at too low flows. In this case, the axial natural frequency of the test system would increase while its damping ratio decreases to eventually produce an unstable operating condition.

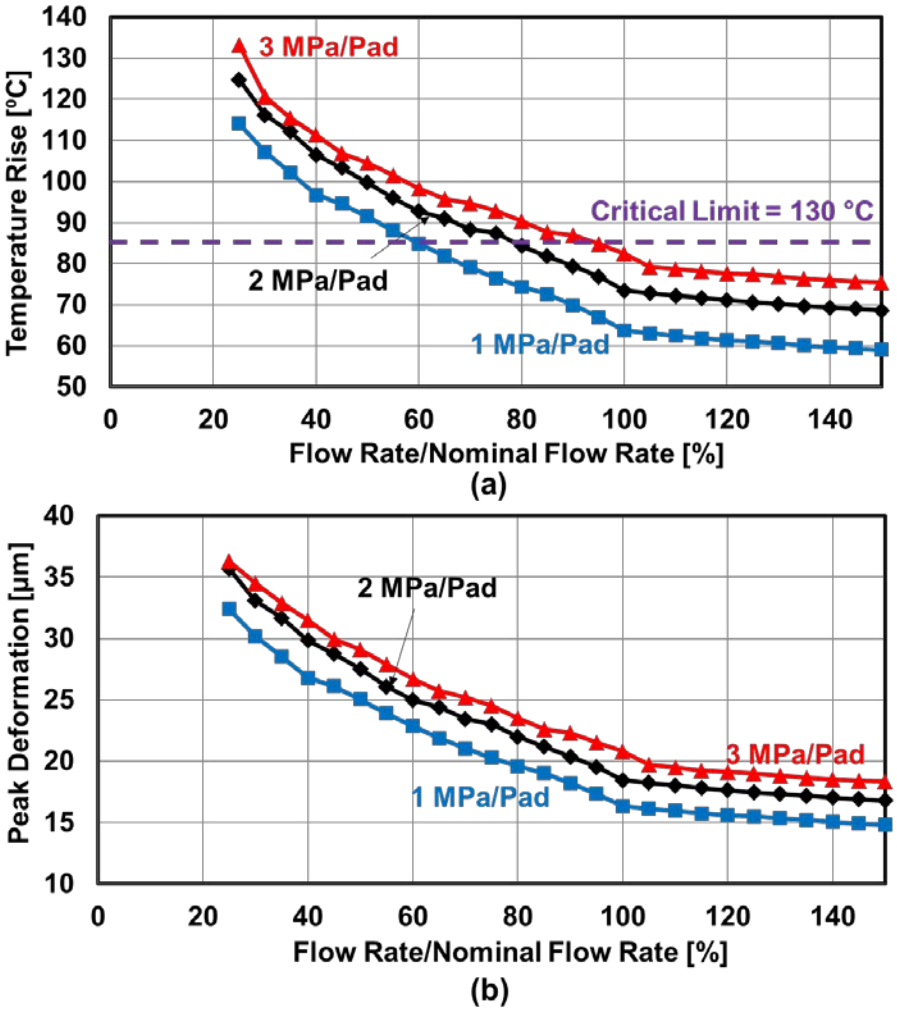

Fig. 14: Predicted (a) peak temperature rise and (b) peak thermal deformation in a pad vs. flow rate and specific load/pad: 1 MPa, 2 MPa, and 3 MPa. Supply temperature = 46 ºC, rotor speed = 4 krpm.

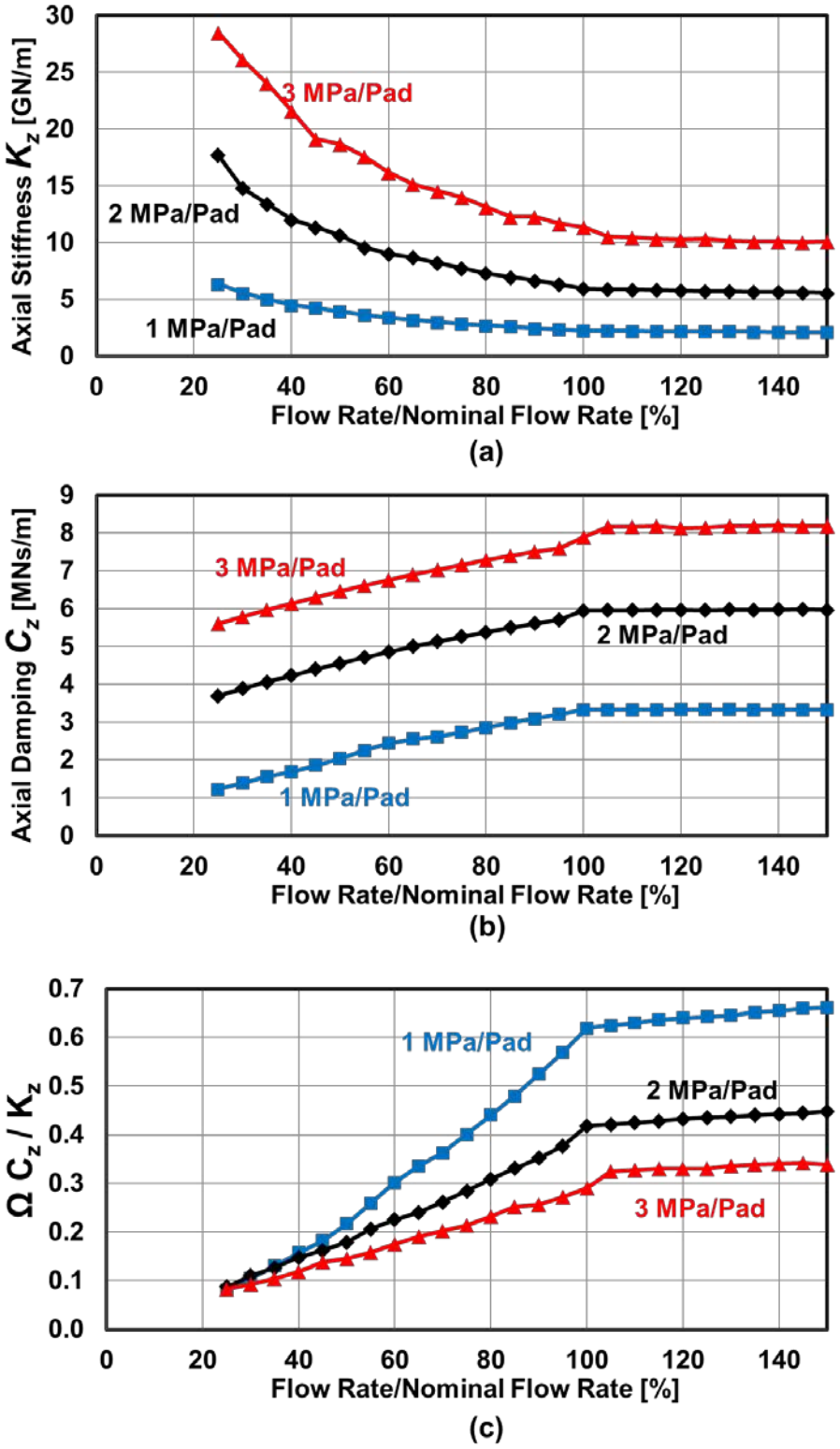

Fig. 15: Predicted fluid film (a) axial stiffness coefficient, (b) axial damping coefficient, (c) ratio ($\Omega C_z/K_z$) vs flow rate and specific load/pad: 1 MPa, 2 MPa, and 3 MPa. Supply temperature = 46 ºC, rotor speed = 4 krpm.

4. CONCLUSION AND PROPOSED FUTURE WORK

Work in 2019/20 integrated a flow starvation model into the XLTHRUSTBEARING® analysis tool to predict the static and dynamic load performance for tilting pad thrust bearing (TPTBs) operating with a reduced flow rate. The inlet flow temperature at a pad leading edge follows from a thermal energy balance in the groove holding an oil bath, and that accounts for the supply flow as well as the hot oil entering the groove from the upstream pad trailing edge. The oil exit temperature and pad subsurface temperature from the current model match measurements for an eight-pad TPTB [23, 7] operating under a specific load/pad ranging from 0.7 MPa to 3.4 MPa and at rotor speeds of 4 krpm and 10 krpm ($R_o\Omega$ = 54 m/s and 135m/s), spanning both laminar flow and fully turbulent flow regimes, respectively. The supply flow rate ranges from 150% to 50% the manufacturer recommended rate.

This report further details characteristic load performance predictions vs supply flow rate ranging from 150% to only 25% of the nominal rate for an identical TPTB operating under 1MPa to 3 MPa specific load per pad and at 4 krpm of rotor speed (surface speed OD). The major findings are:

A supply flow rate exceeding the nominal one (fully wetting the whole pad) produces minimal improvements in pad minimum film thickness or peak temperature rise, whereas the drag power loss constantly increases with the supply flow rate.

a) A flow reduction below the nominal rate produces areas denuded of oil at both the pad leading edge and trailing edge, and thus produces an increase in the peak hydrodynamic pressure while reducing the minimum film thickness. For instance, under a light load, the peak pressure almost doubles and the minimum film thickness decreases by 2/3 as the supply flow rate decreases to 30% of the nominal rate.
b) Under a heavy load of 3 MPa/pad, the pad peak temperature rise exceeds the Babbit critical temperature = 130°C when the supply flow is below 80% of the nominal rate.
c) Compared to a fully flooded operating condition, flow starvation produces a bearing with a larger axial stiffness coefficient but a much lesser axial damping coefficient. In this case, the axial natural frequency of the test system would increase while it's damping ratio quickly decreases to eventually produce an unstable operating condition.

The work here adopts a sound physical model to determine the flow distribution among the bearing pads for operation with a static misalignment. Future work should investigate the

performance of a starved flow thrust bearing operating under thrust collar misalignment. Further, future work could also extend the analysis with more details to differentiate TBs with end seals vs those with evacuated ends.

REFERENCES

[1] San Andrés, L., Koo, B., and Hemmi, M., 2018, "A Flow Starvation Model for Tilting Pad Journal Bearings and Evaluation of Frequency Response Functions: A Contribution Toward Understanding the Onset of Low Frequency Shaft Motions," J. Eng. Gas Turb. Power, **140**(5), p. 052506.

[2] Gregory, R., 1974, "Performance of Thrust Bearings at High Operating Speeds," J. Lub. Tech., **96**(1), pp. 7–13.

[3] Hashimoto, H., 1990, "Performance Characteristic Analysis of Sector-Shaped Pad Thrust Bearings in Turbulent Inertial Flow Regime Under Three Types of Lubrication Conditions," J. Tribol., **112**(3), pp. 477–484.

[4] Abdollahi, B., and San Andrés, L., 2019, "Improved Estimation of Bearing Pads' Inlet Temperature: A Model for Lubricant Mixing at Oil Feed Ports and Validation against Test Data," J. Tribol., **141**(3), p. 031703.

[5] Bielec, M.K. and Leopard, A.J., 1969, "Tilting Pad Thrust Bearings: Factors Affecting Performance and Improvements with Directed Lubrication" Inst. Mech. Eng., **184**(12), pp. 93-102, London, England.

[6] The citation shuld be San Andres, L., Hardik, J., Kaizar, H., and Thorat, M., 2020, "On the Effect of Supplied Flow Rate to the Performance of a Tilting-Pad Journal Bearing. - Static Load and Dynamic Force Measurements," ASME Paper GT2020-16215 (accepted for journal publication).

[7] Capitao, J. W., Gregory, R. S., and Whitford, R. P. 1976, "Effects of High-Operating Speeds on Tilting Pad Thrust Bearing Performance," ASME. J. of Lubrication Tech., **98**(1), pp 73–79. https://doi.org/10.1115/1.3452779

[8] Artiles, A., and Heshmat, H., 1987, "Analysis of Starved Thrust Bearings Including Temperature Effects," J. Trib., **109**(3), pp. 395–401.

[9] Glavatskih, S. B., Fillon, M., and Larsson, R. 2001, "The Significance of Oil Thermal Properties on the Performance of a Tilting-Pad Thrust Bearing," ASME. J. Tribol. **124**(2), pp. 377–385. https://doi.org/10.1115/1.1405129.

[10] Wasilczuk, M. and Rotta, G., 2008, "Modeling Lubricant Flow between Thrust Bearing Pads," Tribol. Intern., **41**(10), pp.908-913. https://doi.org/10.1016/j.triboint.2007.11.007.

[11] DeCamillo, S.M., 2014, "Axial Subsynchronous Vibration," 43rd Turbomachinery & 30th Pump Users Symposia (Pump & Turbo 2014), Texas A&M University. September 23-25, Houston, TX. http : / /hdl .handle .net /1969 .1 /162696.

[12] DeCamillo, S. M., He, M., Cloud, C. H., and Byrne, J. M., 2008, "Journal Bearing Vibration and SSV Hash," 37th Turbomachinery Symposium, Houston, TX, Sept. 7–11.

[13] He, M., Allaire, P., Barrett, L., and Nicholas, J., 2005, “Thermohydrodynamic Modeling of Leading-Edge Groove Bearings Under Starvation Condition,” Tribol. Trans., 48(3), pp. 362–369.

[14] Heshmat, H., and Pinkus, O. 1985, “Performance of Starved Journal Bearings With Oil Ring Lubrication,” ASME. J. Tribol., **107**(1), pp. 23–31. https://doi.org/10.1115/1.3260998.

[15] Ettles, C., 1970, “Hot Oil Carry-Over in Thrust Bearings,” Proc. Instn Mech Engrs, Industrial Lubrication and Tribology, **184**(12) pp. 69-81.

[16] Jeng, M. C., Zhou, G. R., and Szeri, A. Z., 1986, “A Thermohydrodynamic Solution of Pivoted Thrust Pads : Part I — Theory,” J. Tribol., **108**, pp. 195–207.

[17] Almqvist, T., Glavatskih, S. B., and Larsson, R., 1999, “THD Analysis of Tilting Pad Thrust Bearings - Comparison Between Theory and Experiments, ” J. Tribol., **122**(2), pp. 412–417.

[18] Ng, C. W., 1964, “Fluid Dynamic Foundation of Turbulent Lubrication Theory,” ASLE Trans., **7**(4), pp. 311–321.

[19] San Andrés, L., and Koosha, R., 2018, “A Thermo-Elasto-Hydrodynamic (TEHD) Computational Analysis of Tilting Pad Thrust Bearings: Analytical and FE Pad Structure Models,” **TRC-B&C-01-18**, Annual Progress Report to the Turbomachinery Research Consortium, Texas A&M University, College Station, USA., May 15-17. http://hdl. handle .net/ 1969.1/175255.

[20] Brockett, t. S., 1995, “Thermoelastohydrodynamic Lubrication in Thrust Bearings,” PhD Dissertation, University of Virginia, Charlottesville, VA, USA.

[21] San Andrés, L., and Koosha, R., 2017, “Thermo Hydrodynamic (THD) Computational Analysis For Tilting Pad Thrust Bearings (TPTBs),” **TRC-B&C-05-17**, Annual Progress Report to the Turbomachinery Research Consortium, Texas A&M University, College Station, USA., May 21-23. http://hdl .handle .net /1969 .1 /175131.

[22] Henry, Y., Bouyer, J., and Fillon, M. 2014, “An Experimental Hydrodynamic Thrust Bearing Device and Its Application to the Study of a Tapered-Land Thrust Bearing,” ASME. *J. Tribol*. *136*(2), p. 021703. https://doi.org/10.1115/1.4026080.

[23] Mikula, A. M., 1986, “Evaluating Tilting Pad Thrust Bearing Operating Temperatures,” J. Tribol., 29(2), pp. 173–178.

[24] Glavatskih, S.B. and Fillon, M., 2006, “TEHD Analysis of Thrust Bearings with PTFE-Faced Pads”. J. Tribol., 128(1), pp.49-58.

[25] Koosha, R. and San Andrés, L., 2019. “Effect of Pad and Liner Material Properties on the Static Load Performance of a Tilting Pad Thrust Bearing,” J. Eng. Gas Turb and Power, **141**(12), p. 121007. https://doi.org/10.1115/1.4045278.

[26] Guo, A., Wang, X., Jin, J., Hua, D. Y., and Hua, Z., 2015, “Experimental Test of Static and Dynamic Characteristics of Tilting Pad Thrust Bearings,” J. Adv. Mech. Eng., **7**(7), pp. 1-8.

[27] He, M., Bryne, J. M., and Armentrout, R. W., 2018, “Fundamentals of Fluid Film Thrust Bearing Operation and Modeling,” II *Asia Turbomachinery & Pump Symposium*, Suntec, Singapore, 13-15 March; http://hdl.handle.net /1969.1 /172449.

[28] Freeman, J.R. and Woodward, R.W., 1921, Some Properties of White Metal Bearing Alloys at Elevated Temperatures, 188, Govt. Print. Off, Washington, USA.